ACS Infectious Diseases

pubs.acs.org/journal/aidcbc

Article

Open Access

This article is licensed under CC-BY 4.0

Second Generation of 2,2′-Di(indol-3-yl)ethanamines as Antileishmanial Agents: Phenotypic Hit Identification and Pharmacophore Studies

Gian Marco Elisi, Antonio Gkoutzamanis, Sara Maestrini, Cécile Exertier, Michela Eleuteri, Marina Naldi, Alessia Peluso, Miriam Gómez-Benmansour, Aurora Diotallevi, Michele Verboni, Laura Goracci, Manuela Bartolini, Giovanni Bottegoni, Paula Kiuru, Andrea Ilari, Luca Galluzzi, and Simone Lucarini*

Cite This: *ACS Infect. Dis.* 2026, 12, 3028−3042

Read Online

ACCESS | Metrics & More | Article Recommendations | Supporting Information

ABSTRACT: The urgent need for new antileishmanial drugs persists due to resistance and toxicity associated with current treatments. Although bisindoles represent a promising chemotype, our first-generation 2,2′-di(indol-3-yl)-ethanamines, inspired by a natural marine alkaloid, displayed significant cytotoxicity despite potent activity against *L. infantum*. To address this limitation, we designed and synthesized a second-generation series in which the indole bromine substituents were removed, and *N*-methylation was prioritized as a strategy to mitigate cytotoxicity. Compounds **1e**, **2b**, **2f**, **3d**, and **3e** emerged as promising hits, exhibiting potent activity against *L. infantum* promastigotes (IC_{50} = 0.6−3 μM) and markedly improved selectivity indices (SI = 11−66) in THP-1 cells. These compounds retained efficacy in an *in vitro* infection model, with **1e**, **2b,** and **2f** displaying IC_{50} values below 10 μM against intracellular amastigotes. A pharmacophore model derived from URB1483 and **2f** was generated to explore plausible mechanisms of action underlying the antileishmanial activity, with trypanothione reductase (TR) selected as a possible biological target. While compound **2f** showed only weak inhibition (IC_{50} = 71 μM), this could provide a starting point for the structure-based design of future antileishmanial agents. Preliminary ADME-related evaluations of **1e** and **2f** revealed improved aqueous solubility, alongside favorable chemical and metabolic stability specifically for **1e**. Consequently, while **2f** could be a new hit for a still underexploited target, compound **1e** emerges as the most balanced lead candidate for future development of antileishmanial derivatives.

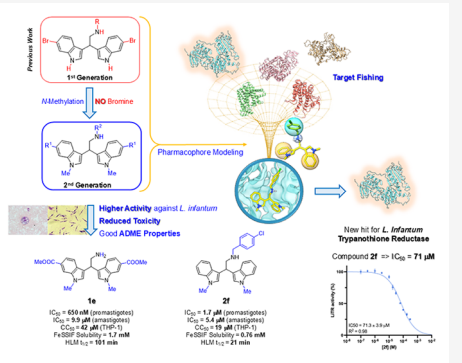

KEYWORDS: *neglected tropical disease, Leishmania, bisindoles, trypanothione reductase, drug discovery*

INTRODUCTION

Leishmaniasis is a major parasitic disease that affects millions of people worldwide, with a disproportionate burden in low-income and resource-limited settings.[1−3] The disease is endemic in tropical areas of Africa, the Middle East, South America, and Asia,[4] and recently, it has expanded to southern Europe, mainly due to global warming, low-cost air links, frequent trade (exchange of goods) between continents, and population migrations.[5,6]

Leishmaniasis is caused by several species of the protozoan *Leishmania*, which are transmitted to mammalian hosts, including humans, by the bite of infected phlebotomine sandflies. Visceral leishmaniasis (VL), one of its clinical manifestations, is the most dangerous, affecting bone marrow, liver, and spleen, and can be fatal if untreated.[7] Cutaneous leishmaniasis (CL), the most common pathological condition, and VL are prevalent in the Mediterranean basin and are caused by *L. infantum* species.[7,8]

Despite recent progress in vaccine research and development, no field-applicable vaccine is available yet,[9] therefore limiting disease management to vector control and chemotherapy.[10] However, commercial drugs have several limitations, ranging from toxicity to drug resistance.[10] Therefore, some research groups, mainly in academia, have discovered new potential drug candidates against leishmaniasis containing privileged heterocycle scaffolds.[11−16] In this context, a few bisindoles have been reported as potential lead compounds against leishmaniasis,[17−22] and in particular, our group has focused on the development of 2,2′-di(indol-3-yl)ethanamine derivatives (Figure 1).[23−25]

Received: January 28, 2026
Revised: July 13, 2026
Accepted: July 28, 2026
Published: August 24, 2026

© 2026 The Authors. Published by American Chemical Society

Downloaded from pubs.acs.org/aidcbc/article-pdf/12/9/3028/6733857/acsinfecdis.6c00079.pdf by UNIV DEGLI STUDI DI URBINO user on 15 September 2026

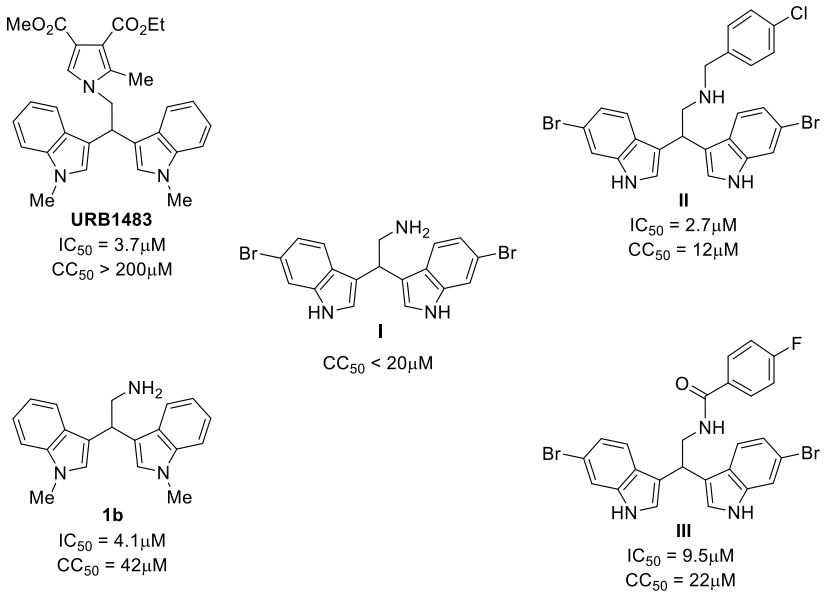

Figure 1. Representative 2,2′-di(indol-3-yl)ethanamine derivatives, a class of bisindoles with antileishmanial activity. Reported IC_{50} were retrieved on *L. infantum* promastigotes and determination of CC_{50} were carried out on human macrophage-like THP-1 cells.

URB1483 (Figure 1), bearing indolyl *N*-Me moieties and no bromine atoms, was the first bisindole reported by our group and showed good potency against *L. infantum* promastigotes (IC_{50} = 3.7 μM) and intracellular amastigotes with no quantifiable cytotoxicity in mammalian cells (SI > 55).[23] However, URB1483 failed during *in vivo* studies on a mouse infection model probably due to its poor water solubility.[24] Consequently, we designed and synthesized more hydrophilic bisindoles, leading to the first generation of 2,2′-di(indol-3-yl)ethanamine derivatives. Compound **II** (Figure 1) was the most potent against *L. infantum* promastigotes with IC_{50} = 2.7 μM. However, **II** was toxic to human macrophage-like THP-1 cells (CC_{50} = 11.7 μM) thus showing a low selectivity index (SI ≈ 4).[24] Another interesting example of this class is the amide **III** (Figure 1), which is active (IC_{50} < 10 μM) but relatively toxic (CC_{50} = 22 μM).[24] Moreover, the marine bisindole alkaloid 2,2′-bis(6-bromo-1*H*-indol-3-yl)ethanamine **I** (Figure 1) was also active against *L. infantum* but toxic (CC_{50} < 20 μM).[24] We speculated that toxicity of compounds **I**, **II** and **III** arises from the presence of bromine atoms on the indole rings (Figure 1), as suggested by comparison with structurally related bisindoles. In addition, *N*-methylation of the indole NH was expected to mitigate the toxic effects on human cells, as observed for URB1483 and compound **II** (Figure 1). Specifically, data obtained for the natural marine alkaloid **I** and its modified analogue **1b** (reported as compound 1h in the previous work)[24] further support this hypothesis. Notably, **1b**, lacking bromine atoms and featuring *N*-methylated indole nitrogens, retained good antileishmanial activity (IC_{50} = 4.1 μM) while displaying markedly reduced cytotoxicity (CC_{50} = 42 μM).[24]

With this in mind, in this work, we designed and synthesized a second generation of 2,2′-di(indol-3-yl)ethanamine derivatives bearing methylated indole nitrogen (*N*-Me) and lacking bromine substitutions on position 6 from the most promising derivatives of our previous work.[24] This new small library was phenotypically screened for efficacy against *L. infantum* promastigotes, and for toxicity on human macrophage-like cells, and a few new compounds showed high potency with very low toxicity and were advanced to the evaluation of their activity in an *in vitro* infection model (intracellular amastigotes).

While some bisindole derivatives exhibit antileishmanial activity through topoisomerase IB inhibition,[17,18,22] the mechanism underlying the antiproliferative effect of 2,2′-di(indol-3-yl)ethanamine derivatives remains unclear. Without a molecular target associated with this biological activity, structure-based studies usually employed to guide ligand design and optimization cannot be leveraged. Therefore, in these circumstances, pharmacophore modeling relying on ligand conformation analysis of potential bioactive geometries, which are often energetically accessible in solution, was carried out.[26,27] Evaluating the accessible conformations of URB1483 and of a representative 2,2′-di(indol-3-yl)ethanamine derivative, a pharmacophore model was generated based on the spatial arrangement of the indole rings and functional groups belonging to the distal portion of the molecules. Alternative conformations were retained in the analysis based on their potential energy. Adopting this approach, we were able to screen previously reported inhibitors associated with a target-mediated inhibition of *L. infantum* proliferation. Our efforts led to a subsequent hypothesis for a potential mechanism of action contributing to the antileishmanial activity of bisindole derivatives. Notably, top-scoring compounds identified through pharmacophore screening, along with the fitting of our compounds within the catalytic site, suggested trypanothione reductase (TR) as a putative target potentially involved in the antileishmanial activity. TR is directly responsible for keeping trypanothione in the reduced state (redox homeostasis), a key enzyme in the redox metabolism, it is indeed essential for parasite survival. Moreover, TR is absent in the host, and it can be efficiently addressed by inhibitors.[28] To prove our hypothesis, a few representative and active compounds belonging to the second generation of 2,2′-di(indol-3-yl)ethanamine derivatives were tested against TR. Pleasantly, some of the compounds exhibited a high-micromolar range inhibition of the enzyme. It is worth mentioning that the biological activity of our compounds cannot be

Downloaded from pubs.acs.org/aidcbc/article-pdf/12/9/3028/6733857/acsinfecdis.6c00079.pdf by UNIV DEGLI STUDI DI URBINO user on 15 September 2026

https://doi.org/10.1021/acsinfecdis.6c00079
ACS Infect. Dis. 2026, 12, 3028−3042

Scheme 1. Synthesis of Bisindole Primary Amines 1[a]

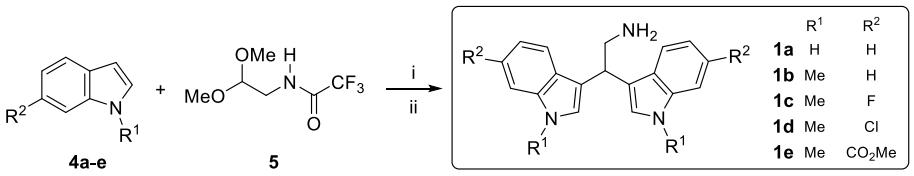

[a]Reagents and conditions: (i) DPP, MeCN, 120 °C, MW, 18 h; (ii) K_2CO_3, MeOH, H_2O, reflux, 1−3 h.

Scheme 2. Synthesis of Bisindole Secondary Amines 2 and Amides 3[a]

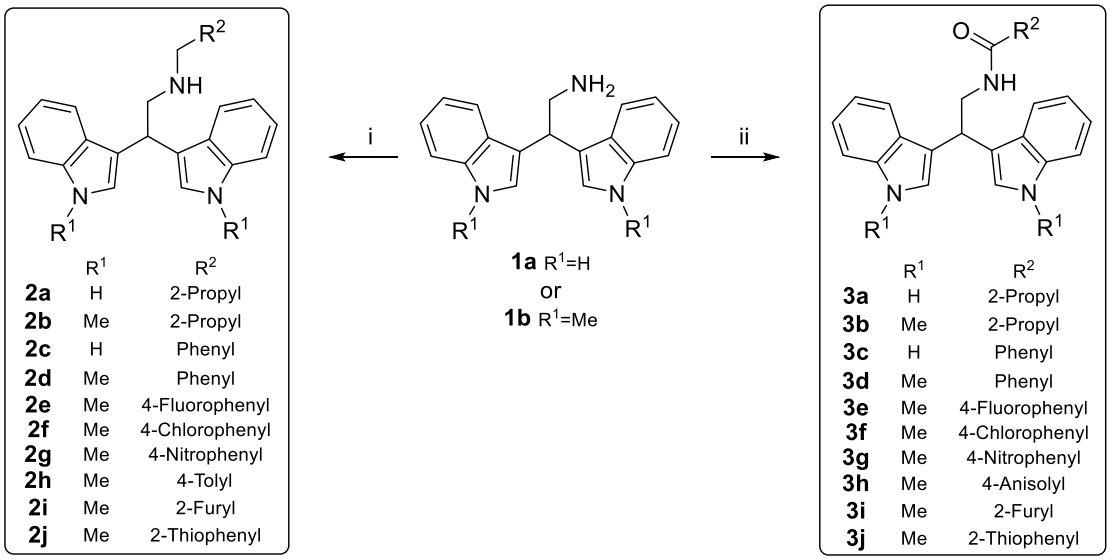

[a]Reagents and conditions: (i) R^2-CHO, $NaCNBH_3$, acetic acid, MeOH, rt, 3−24 h; (ii) R^2-CO_2H, EDC·HCl, DCM, rt, 12 h.

entirely ascribed to this mechanism of action, given also the lack of enzyme inhibition reported for URB1483 and other 2,2′-di(indol-3-yl)ethanamine derivatives, these results could pave the way for the application of bisindole hits in a drug discovery campaign against TR function.

RESULTS

Chemistry

The desired primary amines **1a−e** were obtained via MW-mediated coupling of the appropriate indole **4** and *N*-(2,2-dimethoxyethyl)-2,2,2-trifluoroacetamide **5** in the presence of a catalytic amount of diphenyl phosphate (DPP), followed by the basic hydrolysis of the corresponding bisindole trifluoroacetamide intermediates with potassium carbonate in good overall yields (Scheme 1).[24]

The secondary amine series **2** was synthesized using reductive amination of 2,2-di(1*H*-indol-3-yl)ethanamine (**1a**) or 2,2-bis(1-methyl-1*H*-indol-3-yl)ethanamine (**1b**) in the presence of $NaCNBH_3$ and the appropriate aldehyde (Scheme 2), alkyl, aryl, or heteroaryl groups (Scheme 2; see Supporting Information).[24] Yields from 25% to 89% were obtained for *N*-Me bisindoles **2b, 2d−j**, while the yields of NH bisindoles **2a** and **2c** were 67 and 64%, respectively, significantly higher than the corresponding *N*-methylated bisindoles **2b** and **2d** (28% and 54%).

The amide series **3** was synthesized via amide coupling of the primary amine **1a** or **1b** with the corresponding carboxylic acids in the presence of *N*-(3-(dimethylamino)propyl)-*N*′-ethylcarbodiimide (EDC) hydrochloride (Scheme 2).[24] The (hetero)aryl amides **3** yields were almost quantitative, ranging from 96 to 99%, except for bisindoles **3f** and **3g** with 84 and 91%, respectively. Slightly lower yields were achieved for the isopropylamide derivatives **3a−b** (71 and 84% isolated yields, respectively).

Phenotypic Screening on *L. infantum* Promastigote and THP-1 Cells

The *in vitro* antiparasitic activity of the new bisindole derivatives was first evaluated on *L. infantum* MHOM/TN/80/IPT1 promastigotes at a single dose of 20 μM for 72 h. All the amines **1** and **2** showed antileishmanial activity > 95% (Table 1) and therefore they were all taken into consideration for testing on THP-1-derived macrophages. On the contrary, amides **3** were less active against *L. infantum* promastigotes showing inhibition values lower than 76% at 20 μM and only the two most active bisindoles, **3d** and **3e** (see Table 1, 62.8% and 76.2%, respectively) were tested for toxicity on human THP-1 cells.

Among amines **1** and **2**, seven out of 13 compounds (i.e., **1c**, **1d**, **2a**, **2d−e** and **2g−h**) showed cytotoxicity between 4 and 20 μM and were not included in subsequent experiments. Instead, both amides **3d** and **3e** showed cytotoxicity between 20 and 100 μM and were further studied.

Consequently, eight active and less toxic compounds (i.e., **1e**, **2b−c**, **2f**, **2i−j** and **3d−e**) were tested on *L. infantum* MHOM/TN/80/IPT1 promastigotes for 72 h with scalar dilution 1:2 and 2:3 (from 20 to 0.3 μM) to determine IC_{50} (Figure S1). All eight tested bisindoles showed very good IC_{50} values between 0.7 and 3.4 μM (Table 1). Therefore, the exact

Downloaded from pubs.acs.org/aidcbc/article-pdf/12/9/3028/6733857/acsinfecdis.6c00079.pdf by UNIV DEGLI STUDI DI URBINO user on 15 September 2026

https://doi.org/10.1021/acsinfecdis.6c00079
ACS Infect. Dis. 2026, 12, 3028−3042

Table 1. Summary of Bisindoles Activity on *L. infantum* MHOM/TN/80/IPT1 Promastigotes and THP-1 Cells and Corresponding SIs[a]

Cmpd	Inhibition of *L. infantum* promastigotes at 20 μM (%)	Cytotoxicity on THP-1 cells (100, 20, 4 μM)	*L. infantum* promastigotes IC_{50} (μM) (95% CI)	THP-1 cells CC_{50} (μM) (95% CI)	SI
1a[b]	82.3	20 < CC_{50} < 100	12.9 (11.6−14.6)	n.a.	
1b[b]	98.0	20 < CC_{50} < 100	4.1 (3.7−4.5)	41.6[c]	10.1
1c	99.6	4 < CC_{50} < 20	n.a.	n.a.	
1d	96.8	4 < CC_{50} < 20	n.a.	n.a.	
1e	99.3	20 < CC_{50} < 100	0.65 (0.60−0.71)	42.7 (39.1−45.4)	65.7
2a	99.3	4 < CC_{50}< 20	n.a.	n.a.	
2b	98.8	20 < CC_{50} < 100	1.2 (1.1−1.3)	30.2[c]	25.2
2c	99.6	20 < CC_{50} < 100	1.5 (1.4−1.6)	17.1[c]	11.4
2d	99.5	4 < CC_{50} < 20	n.a.	n.a.	
2e	99.4	4 < CC_{50} < 20	n.a.	n.a.	
2f	98.8	20 < CC_{50} < 100	1.7 (1.6−1.8)	18.7[c]	11.0
2g	95.2	4 < CC_{50} < 20	n.a.	n.a.	
2h	98.2	4 < CC_{50} < 20	n.a.	n.a.	
2i	98.4	20 < CC_{50} < 100	3.2 (3.0−3.4)	30.0[c]	9.4
2j	100.8	20 < CC_{50} < 100	2.8 (2.6−3.0)	26.7[c]	9.5
3a	−34.2	n.a.	n.a.	n.a.	
3b	16.5	n.a.	n.a.	n.a.	
3c	27.6	n.a.	n.a.	n.a.	
3d	62.8	20 < CC_{50} < 100	2.4 (1.9−2.9)	>50[d]	>21
3e	76.2	20 < CC_{50} < 100	3.4 (3.1−3.8)	>100	>29
3f	47.1	n.a.	n.a.	n.a.	
3g	50.9	n.a.	n.a.	n.a.	
3h	41.2	n.a.	n.a.	n.a.	
3i	47.6	n.a.	n.a.	n.a.	
3j	50.7	n.a.	n.a.	n.a.	
MILT	96.8	20 < CC_{50} < 100	3.7 (3.3−4.0)	36.5 (32.8−40.2)	9.9

[a]IC_{50} and CC_{50} values are reported as mean and 95% CI, from at least two independent experiments, each conducted at least in duplicate. Miltefosine (MILT) was used as positive control. n.a. = not available; CI = confidence interval; SI = selectivity index = CC_{50}/IC_{50}. [b]The data were already reported by our group.[24] [c]95% CI was not calculable, see comment in the main text. [d]Precipitation of **3d** at 100 μM occurred.

cytotoxicity (CC_{50}) of the eight compounds was evaluated on THP-1 cells as described in the Methods section. The CC_{50} values ranged from 17.1 to 42.4 μM for amines **1** and **2** (Table 1), including miltefosine, which showed CC_{50} of 36.5 μM. Amides **3d** and **3e** did not induce any appreciable toxicity toward THP-1 cells at concentrations up to 50 and 100 μM, respectively. At higher concentrations, both compounds precipitated in the assay medium, precluding reliable toxicity determination (100 and 200 μM, respectively). Notably, the 95% confidence interval (CI) was not determined for the secondary amines **2** (five compounds). This was due to the steeper slope in dose−response curves that indicate a transition within a very narrow concentration range and high compound potency (Figure S2). Moreover, the discrepancy between the preliminary three-point cytotoxicity range (Table 1, column 3) and the final CC_{50} value (column 5) for these amines stemmed from the more precise calculation afforded by the full dose−response curve. Compound **1e** is the most potent compound against *L. infantum* promastigotes showing a submicromolar IC_{50} against the protozoa (650 nM), together with a low toxicity on THP-1 cells (42.7 μM), therefore resulting in the highest SI (65.7), 6-fold higher than that of miltefosine (Table 1). Finally, based on these results, the compounds **1e**, **2b**, **2f**, **3d** and **3e** were selected for testing in intracellular amastigotes.

Antiamastigote Assay on *L. infantum*-Infected THP-1 Cells

Following the results obtained in the phenotypic screening, five compounds (**1e**, **2b**, **2f**, **3d**, and **3e**) were selected for evaluation against intracellular amastigotes. Interestingly, both the amines **1e**, **2b** and **2f** and the amides **3d** and **3e** were also effective in reducing the infection rate after 72 h of treatment. Among them, the primary amine **1e** emerged as one of the more active compounds, significantly reducing the infection rate at all tested concentrations, with the exception of the treatment at 1.2 μM (Figure 2).

Similarly, the secondary amine **2b** significantly reduced the rate of infection at all the concentrations tested, although significant differences were observed between the treatments 1.2, 2, 5 μM and 10, 15, 20 μM (Figure 2). The other secondary amine, compound **2f**, altered the rate of infection in a dose-dependent manner, with a significant effect observed at 15 μM (Figure 2). No data were reported at 20 μM for this compound due to its cytotoxicity at this concentration, which leads to unreliable results. Microscopic analysis of the infection model further confirmed the cytotoxic effect of compound **2f** on THP-1 cells at the highest tested concentration (i.e., 20 μM) as evidenced by the marked reduction of the number of cells upon treatment (Figure S3). Concerning the amides, compound **3d** significantly reduced infection at 10, 15, and 20 μM concentrations. Similarly, **3e** significantly reduced infection although no statistically significant difference was observed at the highest concentration (Figure 2).

From these data points, IC_{50} values were evaluated for all tested compounds. Interestingly, amines **1e**, **2b** and **2f** displayed IC_{50} values below 10 μM against intracellular amastigotes. Overall, despite their promising efficacy, none of

Downloaded from pubs.acs.org/aidcbc/article-pdf/12/9/3028/6733857/acsinfecdis.6c00079.pdf by UNIV DEGLI STUDI DI URBINO user on 15 September 2026

https://doi.org/10.1021/acsinfecdis.6c00079
ACS Infect. Dis. 2026, 12, 3028−3042

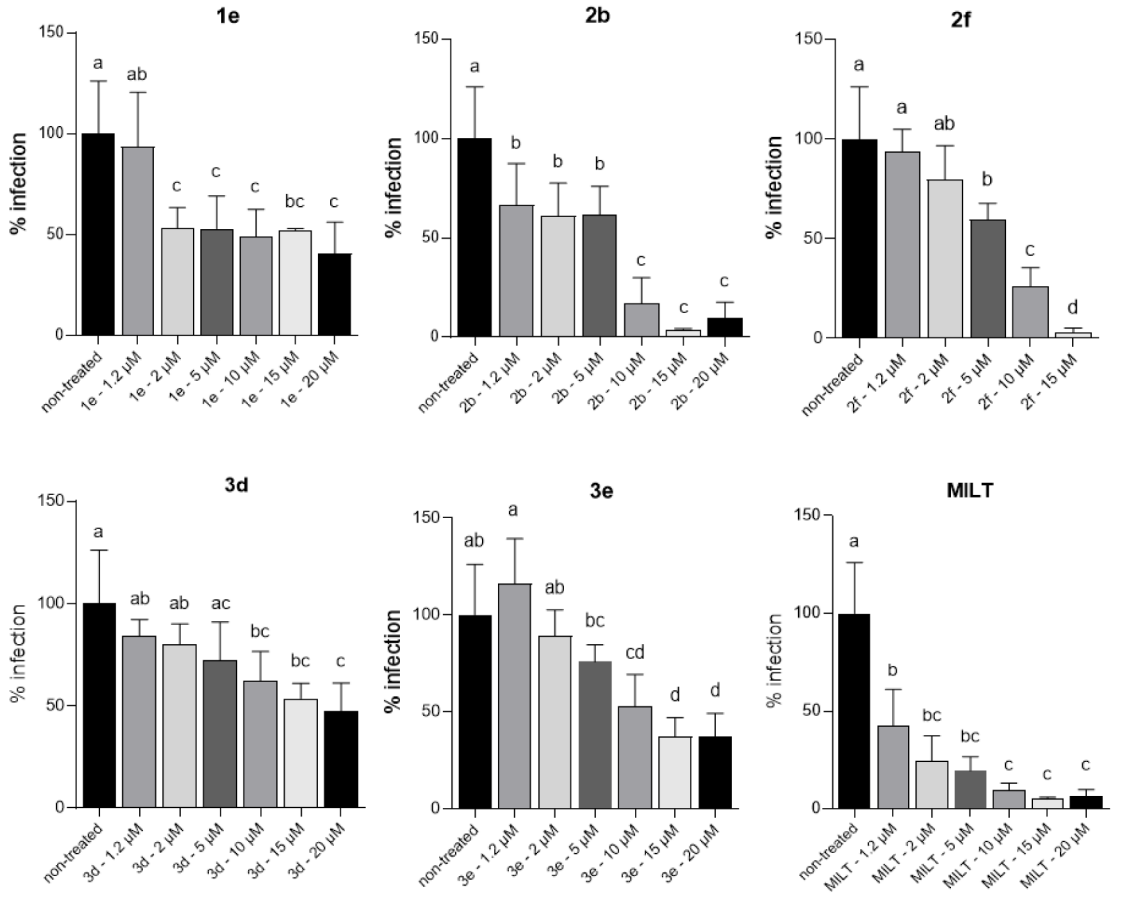

	1e	2b	2f	3d	3e	MILT
IC_{50} on intracellular amastigotes	9.9	3.3	5.4	18.6	11.7	0.6
95% CI	5.4 to 28.6	2.6 to 4.1	4.6 to 6.3	13.6 to 31.0	9.7 to 14.1	0.3 to 1.0

Figure 2. Effect of compounds **1e**, **2b**, **2f**, **3d**, **3e** and miltefosine (MILT) on *L. infantum* intracellular amastigotes. Bar graphs show the percentage of infection in nontreated and following the treatment with increasing concentrations of selected compounds. Data are expressed as mean ± SD. Different letters represent statistically significant differences among the treatments ($p < 0.05$), whereas groups sharing the same letter are not significantly different (ordinary one-way ANOVA with Tukey's multiple comparisons test). The IC_{50} values of all compounds against intracellular amastigotes were calculated by nonlinear regression analysis and expressed as mean and 95% confidence interval.

these compounds reached the potency of the reference drug miltefosine.

Pharmacophore Modeling and Screening of Bisindole Derivatives

Considering common structural features shared between azole-bisindole and 2,2′-di(indol-3-yl)ethanamine derivatives, URB1483 and **2f** were selected to construct a pharmacophore model encompassing putative key determinants of biological activity. The compounds were selected among the best out of the two classes reported for their inhibitory activity on promastigote proliferation. In particular, compound **2f** recapitulates the chemical features common to the most active 2,2′-di(indol-3-yl)ethanamine derivatives. Compound **2f** was analyzed in both its neutral and protonated forms, since both are considered accessible at physiological pH values. This assumption is supported by density functional theory calculations predicting a pK_a of 7.4 for the secondary amine of **2f**.

Potential energy surfaces were generated by analyzing the rotation of torsions τ_1 and τ_2 (Figure 3, left). Conformations of URB1483 and neutral **2f** were compared (Figures S4 and S5) by retaining minima within 2 kcal·mol^{-1} of the global minimum, considering τ_1 and τ_2 values and aromatic ring centroid distances (Figure S6). Among five common potential energy minima, two conformations displayed a symmetrical distribution of pharmacophore features, leading to a final model with four alternative pharmacophore site arrangements (Figure 3, right).

Each pharmacophore model comprises five sites: two representing the bisindole core and three corresponding to the distal portion of the molecules (Figure 4), as detailed in the Methods section. While the orientation of the aromatic rings in the core region (*aro1* and *aro2* sites) is determined by the conformational analysis and accounted for in the pharmacophore model, the optional aromatic sites (*nd-aro1* and *nd-aro2* sites) were not assigned directionality when the pharmacophore scoring function was applied. An additional site (*pos1* site) accounts for a potential feature representing the possibly charged amine group of the bisindole derivatives.

The pharmacophore models were tested for their ability to discriminate known active compounds from decoys (Figure S7), resulting in pharmacophore model **IV** displaying the

Downloaded from pubs.acs.org/aidcbc/article-pdf/12/9/3028/6733857/acsinfecdis.6c00079.pdf by UNIV DEGLI STUDI DI URBINO user on 15 September 2026

https://doi.org/10.1021/acsinfecdis.6c00079
ACS Infect. Dis. 2026, 12, 3028−3042

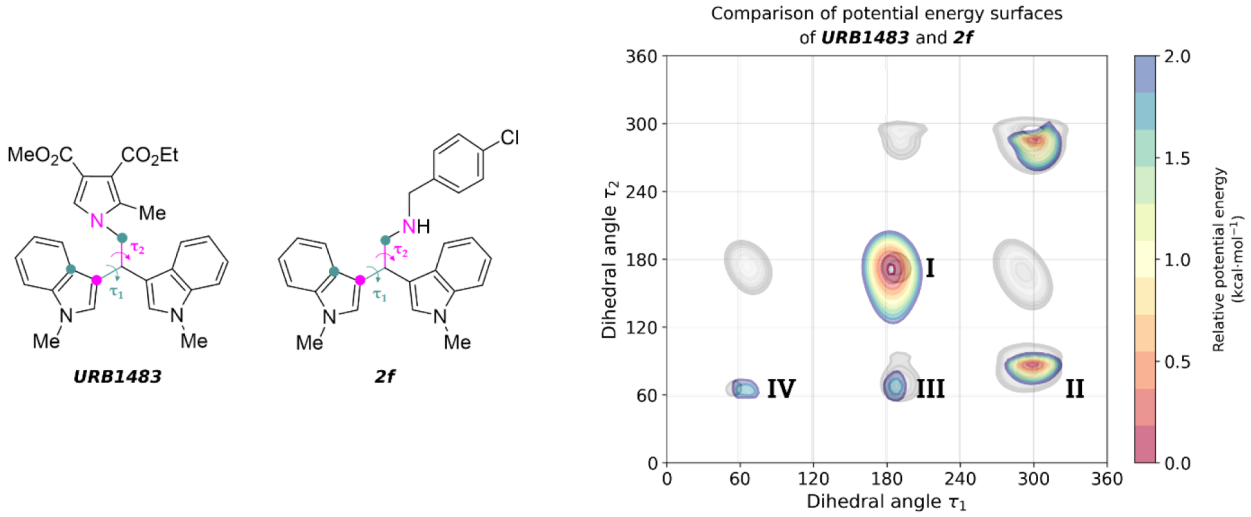

Figure 3. Left: definition of dihedral angles τ_1 and τ_2 for the calculation of potential energy surfaces of URB1483 and **2f**. Right: superposition of the potential energy surfaces of URB1483 (in colormap) and **2f** in its neutral state (in gray colormap). Common potential energy minima associated with their respective pharmacophore models are marked with Roman numerals.

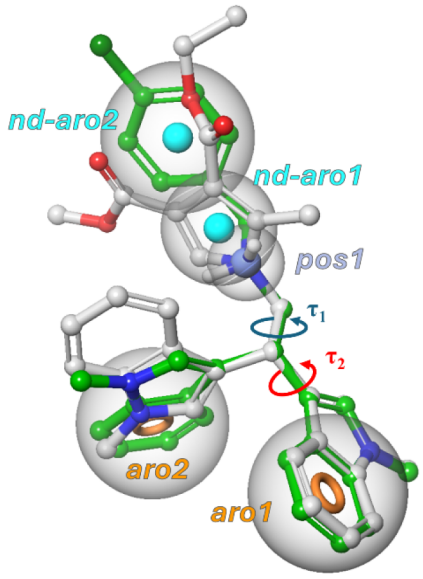

Figure 4. Representative conformations of URB1483 (white sticks) and **2f** (green sticks) aligned on pharmacophore model **I**. Pharmacophore features comprised in the pharmacophore model account for aromatic sites (*aro1* and *aro2* in orange) that position bisindole rings. Other features describe the functional groups belonging to the distal region of the ligands: the presence of a positive net charge (*pos1* site, blue sphere) and of aromatic rings (*nd-aro1* and *nd-aro2* sites, cyan spheres) of the two series of compounds considered in pharmacophore building.

highest discriminative power in receiver operating characteristic (ROC) curve analysis. The models were subsequently used for screening a library of compounds extracted from the ChEMBL34 database[29] and annotated for biological activity against *Leishmania* spp. (Figures S8–S9). Across all four independent runs with the alternative pharmacophore models, five compounds reported by Chauhan et al.[30] and bearing a β-carboline–quinazolinone scaffold consistently achieved a high pharmacophore fitness score (Table S1, Figures S10–S11). These compounds were reported to exhibit against *L. donovani* TR a low-micromolar activity, i.e., relatively good potency considering the challenges involved in achieving high enzyme inhibition for TR inhibitors.[28,31]

Evaluation of TR Enzymatic Inhibition

A selection of five promising bisindoles, together with URB1483, were tested at 10 μM to evaluate their ability to inhibit *L. infantum* trypanothione reductase (LiTR) activity (Figure S12). Specifically, no inhibition of LiTR activity was observed for the primary amines **1b** and **1e** and URB1483, whereas the secondary aliphatic amine **2b** displayed only a minimal effect (3.3% inhibition). Conversely, the secondary aromatic amine **2f** and the amide **3e** significantly inhibited LiTR enzymatic activity. Among these, **2f** emerged as the most potent inhibitor, reducing LiTR activity to 78.1%. Moreover, its subsequent inhibitory profiling yielded an IC_{50} value of 71.3 ± 3.9 μM at 25 °C (Figure S13).

Bisindole derivatives were docked within the catalytic site of LiTR. Given the shallow nature of the LiTR protein surface and the presence of different subsites, we guided docking calculations using a three-point pharmacophore model built on the putative binding mode of compound **6e** (Table S1), which is the most potent compound belonging to the series of β-carboline–quinazolinone derivatives reported as inhibitors of the *L. donovani* TR orthologue[30] to match the three aromatic sites. Subsequently, the hypothesis for the binding of compound **2f** was generated by recreating the pharmacophore model of 2,2′-di(indol-3-yl)ethanamine derivatives on the protein surface (Figure 5) in order to perform guided docking calculations. According to this model, the two indole rings position close to the catalytic tetrad and the distal aromatic portion would bind a subsite close to the catalytic site at the interface between the two protein subunits. Moreover, the charged amino group is placed near the γ-Glu site, resulting in a reinforced salt-bridge interaction with E467′.

Kinetic Solubility Evaluation of Compounds URB1483, 1e, and 2f

The kinetic solubility of compounds URB1483, **1e** and **2f** was assessed in three different media, phosphate buffer (pH 7.4), fasted-state simulated intestinal fluid (FaSSIF, pH 6.5), and fed-state simulated intestinal fluid (FeSSIF, pH 5.0), at 37 °C, following a protocol previously described[32] with minor

Downloaded from pubs.acs.org/aidcbc/article-pdf/12/9/3028/6733885/7/acsinfecdis.6c00079.pdf by UNIV DEGLI STUDI DI URBINO user on 15 September 2026

https://doi.org/10.1021/acsinfecdis.6c00079
ACS Infect. Dis. 2026, 12, 3028–3042

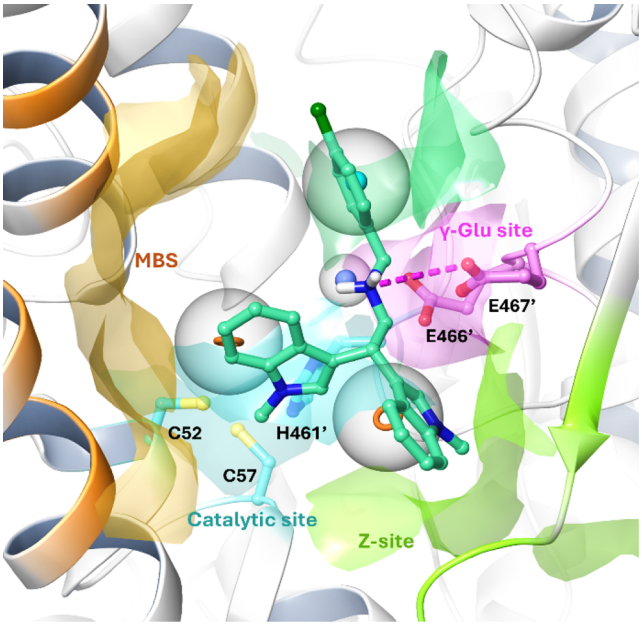

Figure 5. Docking of compound **2f** within the catalytic site of LiTR (PDB code: 4ADW)[47] and fitting with the pharmacophore model. The two aromatic features (orange sites), accommodating bisindole substituents, are close to residues of the catalytic site (cyan) and of the Z-site (green). The secondary amino group, represented as a blue sphere, interacts with E466′ and E467′ (γ-Glu site). The third aromatic group is placed on the optional aromatic site (cyan sphere) close to a cleft between the two protein subunits (green surface).

modifications (see Methods section). Compound URB1483 displayed solubility values below the limit of detection/quantification in phosphate buffer and showed very low solubility in FaSSIF (10.4 ± 0.6 μM) and FeSSIF (89 ± 6 μM). Similarly, compound **2f** exhibited low solubility in phosphate buffer (0.20 ± 0.03 μM) and FaSSIF (3.5 ± 0.7 μM), while a substantially higher solubility was observed in FeSSIF (757 ± 41 μM). Conversely, compound **1e** demonstrated high solubility across all media, with values of 1017 ± 37 μM in phosphate buffer, 796 ± 64 μM in FaSSIF, and 1666 ± 12 μM in FeSSIF. For all compounds, solubility in FeSSIF was consistently higher than in FaSSIF, indicating that the increased concentration of bile salts and lipids in the fed-state medium enhances dissolution. This effect is attributed to the formation of micelles and other colloidal structures capable of solubilizing poorly soluble drugs.

Chemical Stability Studies on Compounds 1e and 2f

For compounds **1e** and **2f**, the chemical stability was investigated in phosphate buffer at pH 7.4, 0.1 M (see Methods section). In this assay, **1e** and **2f** (1 μM with 0.5% DMSO) were incubated at 37 °C in phosphate buffer (pH 7.4), and samples were collected at 0, 15, 30, 45, and 60 min. Each sample was subsequently analyzed by LC-MS. Under these conditions, while compound **1e** showed good chemical stability with a relative area percentage of remaining compound over 95% at 60 min (Figure S14), compound **2f** showed apparent chemical instability as early as 15 min, likely due to its poor solubility in phosphate buffer.

Plasma Stability Studies on Compounds URB1483, 1e, and 2f

Plasma stability studies were performed on compounds **1e** and **2f** together with the reference lead compound URB1483 by incubating the compounds in human plasma at 37 °C for up to 4 h and monitoring the residual parent compound by LC-MS analysis. After 2 h of incubation, all compounds showed high stability with very limited (URB1483) or negligible (**1e** and **2f**) degradation (Table S2). After 4 h, compounds **1e** and **2f** still retained 100% and 98.3% of the parent compound, respectively, whereas the residual amount of URB1483 decreased to 91.9%. For URB1483, LC-MS analysis additionally revealed the presence of two major degradation products, consistent with the hydrolysis of either the methyl ester alone or both the methyl and ethyl ester moieties. These products were absent at t_0 and became detectable only after prolonged incubation. In contrast, no detectable degradation products were observed for compounds **1e** and **2f** under the investigated conditions.

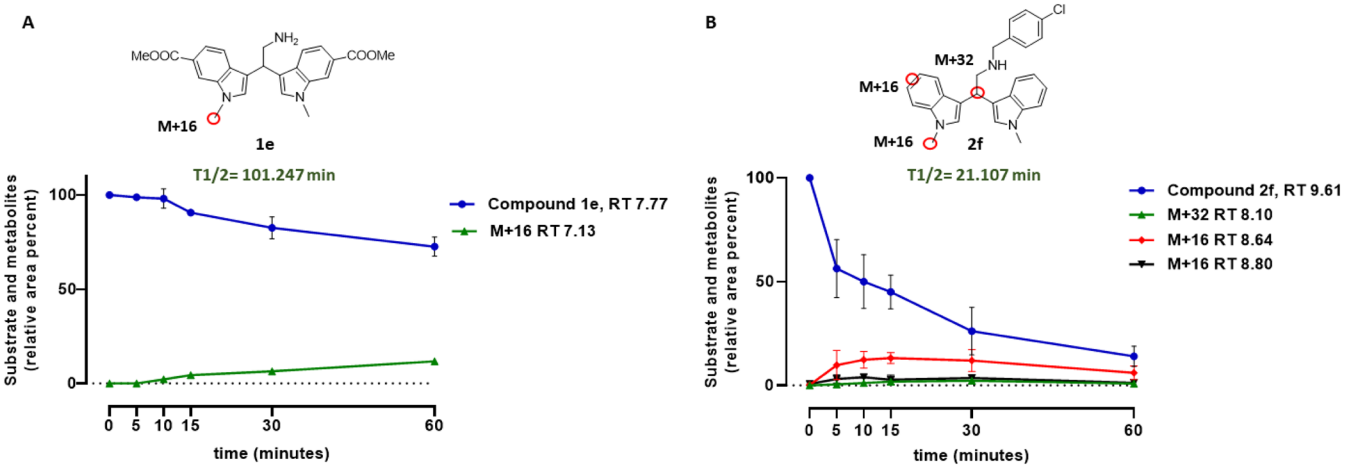

Figure 6. Metabolic stability in HLM of compounds **1e** and **2f** over a 60 min incubation. Chemical structures of compounds **1e** (A) and **2f** (B), respectively, with the liability points (soft spots) related to the sites of metabolism are depicted at the top of each panel. For each compound, the observed behavior for substrate metabolic degradation is shown in blue, while the formation of metabolites, whose names are expressed in relation to the mass variation compared to the substrate, is shown in empty red circles. Data reported in the graph represent the mean ± SD from n = 3 experiments. The half-life values associated with each compound and expressed in minutes are reported in green.

Downloaded from pubs.acs.org/aidcbc/article-pdf/12/9/3028/6733857/acsinfecdis.6c00079.pdf by UNIV DEGLI STUDI DI URBINO user on 15 September 2026

https://doi.org/10.1021/acsinfecdis.6c00079
ACS Infect. Dis. 2026, 12, 3028−3042

Metabolic Stability Studies on Compounds URB1483, 1e, and 2f

For compounds URB1483, **1e** and **2f** (1 μM with 0.5% DMSO) the metabolic stability in human liver microsomes (HLM) at 37 °C was also studied by monitoring the percentage of unmodified compound and the formation of metabolites over a period of 60 min incubation (time points: 0, 5, 15, 30, and 60 min) (Figure 6). It is worth noting that the use of HLM also enabled preliminary assessment of possible esterase-mediated metabolic conversion in addition to oxidative metabolism, as human liver microsomal fractions retain hydrolytic enzyme activities, including carboxylesterases.[33] Samples were analyzed by LC-MS/MS and the raw data were processed by using Mass-MetaSite (Molecular Discovery Ltd.)[34−36] and WebMetabase (Molecular Discovery Ltd.)[37,38] software for automatic metabolite identification and structure elucidation as well as for kinetic analysis. For compound URB1483, a rapid decrease in the parent compound signal was observed over time; however, no metabolites were detected. Control experiments performed in the absence of NADPH showed a comparable decline in compound levels (Figure S15), indicating that the observed decrease was mainly attributable to poor solubility and precipitation in the incubation medium rather than to metabolic conversion. Therefore, reliable assessment of the intrinsic microsomal metabolic stability of URB1483 could not be achieved under the investigated experimental conditions. For compound **1e**, the only detected metabolic transformation involved aliphatic hydroxylation of the *N*-methylindole moiety, and the compound exhibited a half-life of approximately 101.2 min (Figure 6A). By comparison, compound **2f** underwent not only aliphatic hydroxylation of both the *N*-methylindole moiety and the junction between the two heterocyclic rings, but also aromatic hydroxylation on the indole ring, resulting in a markedly shorter half-life of 21.1 min (Figure 6B). This reduced metabolic stability may be attributed, at least in part, to its poor solubility in the incubation medium.

DISCUSSION

Leishmaniasis is a major neglected tropical disease, ranking second only to malaria in parasitic mortality.[9] Owing to global warming and the broader consequences of globalization, its endemic areas are expanding into nontropical regions, including parts of Europe. Despite this urgency, no commercial human vaccine exists, and treatment relies on limited and/or relatively expensive drugs (e.g., amphotericin B, miltefosine). Moreover, the use of these agents is seriously hindered by the occurrence of acute/chronic toxicity and increasing resistance in some *Leishmania* strains. These limitations underscore the urgent need for new, safe, and affordable antileishmanial agents. Among emerging chemotypes, bisindole derivatives have recently gained attention as promising candidates.

In this context, URB1483 (Figure 1) demonstrated efficacy against *L. infantum* promastigotes and intracellular amastigotes, crucially exhibiting no quantifiable cytotoxicity in mammalian cells.[23] However, URB1483 failed *in vivo* studies in a murine infection model, primarily due to poor water solubility and unfavorable physicochemical properties.[24] Consequently, we designed the first generation of 2,2′-di(indol-3-yl)ethanamines based on the natural marine bisindole alkaloid **I** (Figure 1). We speculated that the heightened cytotoxicity against human cells was primarily attributable to the presence of bromine atoms on the indole rings (compounds **I**, **II**, and **III**, Figure 1). Conversely, we hypothesized that methylation of the indole NH group (*N*-Me), as exemplified by URB1483 and compound **1b**, could mitigate the cytotoxic effects of the resulting derivatives on mammalian cell lines. We embarked on the design and synthesis of a second-generation small library of 2,2′-di(indol-3-yl)ethanamine derivatives, prioritizing incorporation of the *N*-methylated indole nitrogen while omitting the 6-bromo substituents, in line with insights gained from the most promising first-generation compounds.[24]

Primary amines **1** were obtained via microwave irradiation (Scheme 1), which facilitated the coupling of the requisite indole **4** and amide **5**, followed by basic deprotection. Secondary amines **2** were synthesized through the reductive amination of the corresponding primary amine **1** and various aldehydes, utilizing $NaCNBH_3$ as the reducing agent. Finally, amides **3** were readily synthesized in good to excellent yields (Scheme 2) from the appropriate primary amines **1** and the opportune carboxylic acid, mediated by the coupling agent EDC.[24]

A phenotypic screening was performed on all 23 synthesized compounds against *L. infantum* promastigotes as a rapid, well-standardized step to identify compounds with potential antileishmanial activity.[39,40] However, it should be noted that results obtained in promastigotes should be interpreted cautiously since activity against this parasite stage does not always correlate with the activity against amastigotes. All primary amines **1** and secondary amines **2** exhibited significant antileishmanial activity, showing >95% inhibition at a concentration of 20 μM. In contrast, only two amides, **3d** and **3e**, displayed sufficient potency at 20 μM to warrant further investigation, achieving 63% and 76% inhibition of the promastigotes, respectively. Consequently, a preliminary cytotoxicity assay was conducted on all amines (**1** and **2**) and the two most promising amides (**3d** and **3e**) using human macrophage-like THP-1 cells. Amines **1c−d**, which bear a halogen substituent on the indole ring (fluorine and chlorine, respectively), were found to be cytotoxic, similar to the natural bisindole **I** (Figure 1) and its *N*-methylated derivative (compound **1i** reported previously).[24] A toxic effect was also observed for the secondary amine **2e**, which contains a fluorine atom in the benzyl ring. Interestingly, the free NH indole amine **2a** was found to be highly cytotoxic, whereas the corresponding *N*-Me derivative **2b** exhibited significantly reduced toxicity (Table 1). This observation supports one of the initial design hypotheses for this second-generation class of compounds.

Accordingly, eight compounds identified as active and exhibiting reduced cytotoxicity (**1e**, **2b−c**, **2f**, **2i−j**, **3d−e**) and the reference drug miltefosine were tested against *L. infantum* promastigotes to determine their inhibitory concentration (IC_{50}) and evaluated for cytotoxicity against THP-1 cells to establish the cytotoxic concentration (CC_{50}). All tested compounds demonstrated excellent potency and reduced cytotoxicity, yielding selectivity index (SI) values ranging from 9.4 to 66. Again, this significant increase in SI confirms the improved design of this second-generation class of compounds compared to the previously reported analogues, which exhibited SI values lower than 10.

Primary amine **1e**, bearing a 6-COOMe substituents, emerged as the most promising compound, exhibiting a potent IC_{50} of 650 nM and an exceptional SI of 66. Among the secondary amines **2**, compound **2b**, which possesses an

Downloaded from pubs.acs.org/aidcbc/article-pdf/12/9/3028/6733857/acsinfecdis.6c00079.pdf by UNIV DEGLI STUDI DI URBINO user on 15 September 2026

https://doi.org/10.1021/acsinfecdis.6c00079
ACS Infect. Dis. 2026, 12, 3028−3042

isopropyl substituent on the ethylamine side chain, demonstrated significant activity with an IC_{50} of 1.2 μM and a good SI of 25. Similarly, good results were obtained for the bisindole **2f**, which showed an IC_{50} of 1.7 μM and an acceptable SI of 11, a value comparable to that of miltefosine (Table 1), despite bearing a 4-chlorobenzylamino substituent. When compared to the corresponding first-generation derivative **II** (Figure 1), **2f** demonstrated superior potency (IC_{50}: 1.7 μM vs 2.7 μM) and reduced cytotoxicity (CC_{50}: 19 μM vs 12 μM) resulting in a nearly 3-fold increase in selectivity (SI: 11 vs 4). Although the benzoic amide **3d** and 4-fluorobenzoic amide **3e** were less potent (IC_{50} values of 2.4 μM and 3.4 μM, respectively), they displayed no cytotoxicity at the tested concentration, resulting in excellent SI values greater than 21 and 29, respectively (Table 1). Again, a comparison with the corresponding first-generation derivative **III** (Figure 1) confirms the design success: bisindole **3e** showed markedly superior potency (IC_{50}: 3.4 μM vs 9.5 μM) and was found to be a nontoxic compound at the tested concentrations (CC_{50}: >100 μM vs 22 μM). Consequently, the selectivity increased more than 15-fold (SI: >29 vs 2).

The five most promising compounds (**1e**, **2b**, **2f**, **3d**, and **3e**), along with miltefosine as a positive control, were selected for further evaluation against *L. infantum* amastigotes within the THP-1 macrophage-like cell line. All tested compounds demonstrated efficacy against the intracellular amastigotes and yielded favorable dose−response curves. Among them, the amines **1e**, **2b**, and **2f** were the most potent, exhibiting IC_{50} values in the low micromolar range (3−10 μM). In contrast, the amides **3d** and **3e** were less potent, displaying IC_{50} values between 10 and 20 μM.

Although 2,2′-di(indol-3-yl)ethanamine derivatives are reported as antileishmanial agents,[24] no clear mechanism behind their biological activity has been revealed. Therefore, we employed a ligand-based virtual screening procedure aiming at target identification. Given the results obtained in the promastigote proliferation inhibition assay, URB1483 and compound **2f** were used to generate a pharmacophore model to screen compounds reported in the literature for their antileishmanial activity. Notably, only compounds exhibiting target-mediated activity were retained in the process to support a plausible mechanism underlying their biological effects. Our virtual screening workflow retrieved trypanothione reductase as a potential target for the bisindole derivatives, based on compounds showing the highest pharmacophore fitness scores.

URB1483 and a few second-generation 2,2′-di(indol-3-yl)ethanamine derivatives (**1b**, **1e**, **2b**, **2f**, **3d** and **3e**) were tested for their ability to inhibit LiTR at a fixed concentration of 10 μM (Figure S12), resulting in compound **2f** emerging as the most potent inhibitor, scoring an IC_{50} of approximately 70 μM. The putative binding mode of compound **2f** (Figure 5), retrieved according to the pharmacophore-guided docking calculations, reveals a Y-shaped occupation of the catalytic site, considering an arrangement of the indolyl substituents closely resembling the requirements of pharmacophore model IV (Figure S6). Guided by docking of compound **6e** (Figure S11), the pharmacophore sites were placed within the binding pocket near the catalytic tetrad. Comparing the results from enzymatic studies and their predicted interactions with the catalytic site, the presence of the distal aromatic ring might be necessary, given the absence of LiTR inhibition reported for compounds **1a**, **1e**, and **2b**, which either lack the terminal portion or present an aliphatic substituent. Moreover, the presence of methyl-ester groups in position 6 of compound **1e** may also create steric clashes with hydrophobic residues belonging to the mepacrine binding site (MBS) or to the Z-site, further supporting the dissociation of the bisindoles' activity observed in the phenotypic screening from LiTR weak engagement. Instead, the importance of the charged amino group present in compound **2f** is also supported by the lower inhibition of enzymatic activity observed with derivatives **3d** and **3e**, when tested at 10 μM concentration. Indeed, the compounds are characterized by an amide group instead of the aliphatic amine, potentially resulting in a decreased interaction with the γ-Glu site. Moreover, the distance of the aromatic site (*nd-aro2*, in Figure 4) relative to the bisindole moiety might also be determinant for the activity. URB1483 lacks the longer and more flexible spacer common to the 2,2′-di(indol-3-yl)ethanamines, resulting in a closer position of its aromatic site relative to the position of bisindoles. Such reduced spacing between the aromatic sites may not be compatible with the protein environment in the catalytic site, resulting in insufficient occupation of the cleft between the two protein subunits potentially causing the lack of activity.

Due to the limited inhibition of enzymatic activity reported for LiTR at the tested concentration (Figure S12) and the inactivity of bisindole derivatives at the enzyme level despite retaining low-micromolar potency in proliferation assays, it can be inferred that the antileishmanial activity of these compounds cannot solely be ascribed to the mechanism identified through our ligand-based virtual screening. Therefore, other targets may still be engaged by our 2,2′-di(indol-3-yl)ethanamine derivatives, either because their known ligands do not meet the pharmacophore requirements or because such targets have not yet been characterized in the context of *Leishmania* spp. proliferation. Nevertheless, compound **2f** could represent a starting point for hit optimization against LiTR, which is a promising but daunting target for the development of antileishmanial agents. Indeed, LiTR is absent in mammals, thereby reducing potential toxicity effects. Furthermore, this target remains largely unexplored, with only a few low-potency inhibitors reported in the literature probably due to the enzyme's shallow druggable pocket.

To support future *in vivo* investigations of the most promising compounds identified in this work, namely **1e** and **2f**, preliminary developability and ADME-related studies were performed. The early integration of such studies represents a strategic choice to avoid "dead-end" hit compounds with high potency but poor drug-like properties, as previously encountered with URB1483. Amides **3d** and **3e** were omitted from the current study owing to the solubility limitations observed during preliminary biological assays. Secondary amine **2f** exhibited poor kinetic solubility in neutral media, showing values of 0.20 μM in phosphate buffer and 3.5 μM in FaSSIF. Conversely, a markedly higher solubility was observed in FeSSIF (757 μM), corresponding to an approximately 8-fold increase relative to the reference compound URB1483 (89 μM). In contrast, primary amine **1e** displayed consistently high solubility across all tested media, with values of approximately 1 mM in phosphate buffer, 0.8 mM in FaSSIF, and 1.7 mM in FeSSIF. Chemical stability in phosphate buffer at physiological pH could be successfully assessed for compound **1e**, which remained stable throughout the entire incubation period, whereas for compound **2f**, the low aqueous solubility precluded a reliable evaluation of chemical stability under the same experimental conditions.

Downloaded from pubs.acs.org/aidcbc/article-pdf/12/9/3028/6733857/acsinfecdis.6c00079.pdf by UNIV DEGLI STUDI DI URBINO user on 15 September 2026

https://doi.org/10.1021/acsinfecdis.6c00079
ACS Infect. Dis. 2026, 12, 3028−3042

Since compound **1e** contains an ester functionality potentially susceptible to hydrolysis, and since plasma stability represents an important component of early ADME profiling beyond esterase-mediated degradation alone, plasma stability of compounds **1e** and **2f** in human plasma was assessed using an LC-MS-based workflow, which enabled both quantitative monitoring of the parent compounds and detection of possible degradation products. In parallel, the plasma stability of the reference lead compound URB1483 was also assessed. Plasma incubation experiments were conducted at 37 °C over a 4 h period, representing a relatively stringent time window commonly employed in early ADME profiling to assess susceptibility to plasma-mediated degradation. Under these conditions, compounds **1e** and **2f** showed high plasma stability, with no significant degradation after 4 h incubation. In contrast, URB1483 showed detectable, although limited, degradation, with 91.9% of the parent compound remaining after 4 h of incubation and the appearance of hydrolytic degradation products attributable to partial ester cleavage.

The high plasma stability observed for **1e** and **2f** indicates that these compounds are unlikely to undergo extensive plasma-mediated hydrolysis during the early stages of systemic exposure. Although plasma stability data alone do not establish the molecular species responsible for the antileishmanial activity observed *in vitro*, the overall stability profile of compound **1e**, including its chemical stability at physiological pH and resistance to plasma-mediated hydrolysis, suggests that the parent compound remains largely intact during the time frame relevant to the biological assays. Therefore, while a contribution from hydrolytic products cannot be formally excluded, the available data do not support extensive hydrolysis as the predominant determinant of the observed biological activity. Consistent with this interpretation, we previously demonstrated that the diacid hydrolysis product derived from URB1483 does not inhibit promastigote proliferation (data not shown). Although this metabolite is not identical to the putative hydrolysis product of **1e**, these findings are in line with the expectation that conversion of these bisindole esters into the corresponding diacid forms may substantially reduce membrane permeability owing to extensive ionization at physiological pH, thereby limiting intracellular target engagement.

Regarding metabolic stability in HLM, compound **1e** exhibited an excellent half-life ($t_{1/2}$) of approximately 100 min. The only detected metabolite was the *N*-hydroxymethylindole derivative (Figure 6, Panel A). In comparison, compound **2f** underwent more extensive metabolism (Figure 6, Panel B), showing a less favorable stability profile with a $t_{1/2}$ of approximately 20 min.

Taken together, these early developability studies indicate that second-generation optimization successfully improved several ADME-related properties relative to URB1483, particularly for compound **1e**, which combines potent antileishmanial activity with markedly enhanced aqueous solubility and favorable chemical, plasma, and microsomal stability profiles. Although these data do not yet define a fully optimized pharmacokinetic profile, they support the further development of **1e** as a promising lead candidate for future *in vivo* evaluation.

CONCLUSIONS

In this study, we designed and synthesized a second-generation series of 2,2′-di(indol-3-yl)ethanamines by removing the indole bromine substituents and prioritizing *N*-methylation, starting from previously reported first-generation hit compounds. This rational modification strategy successfully reduced cytotoxicity while preserving antileishmanial potency. In detail, **1e**, **2b**, **2f**, **3d**, and **3e** emerged as promising hits, displaying potent activity against *L. infantum* promastigotes and markedly improved selectivity indices in THP-1 cells, thereby validating our design hypothesis. Importantly, these compounds retained efficacy in an *in vitro* infection model, with compounds **1e**, **2b** and **2f** identified as the most potent bisindoles against intracellular amastigotes.

Ligand-based pharmacophore modeling and target-oriented virtual screening identified TR as a plausible molecular target for this compound class. Consistent with this hypothesis, the representative derivative **2f** inhibited the purified enzyme, albeit with weaker inhibition (IC_{50} = 71 μM) than that reasonably required to elicit the antileishmanial activity reported in the phenotypic screening. While this level of enzyme inhibition clearly suggests the involvement of additional molecular targets, the pharmacophoric features and the identification of hotspot interactions with TR offer a potential starting point for the future design of compounds targeting redox metabolism in *Leishmania* species.

Preliminary developability and ADME-related studies highlighted compound **1e** for its superior aqueous solubility and chemical and metabolic stability, supporting its progression as the primary lead candidate. Overall, these results establish N-methylated, nonbrominated bisindoles as a promising scaffold for the development of safer and more effective antileishmanial agents with an improved ADME profile.

MATERIALS AND METHODS

Chemistry

Materials are reported in the Supporting Information.

Synthesis of Bisindole Primary Amines 1

The (trifluoroacetylamino)acetaldehyde dimethyl acetal **5** (1.3 mmol, 1 equiv) was dissolved in dry acetonitrile (1 mL per 1 mmol) in a MW tube under argon atmosphere. To the solution was added the appropriate indole **4a−e** (2 equiv) and DPP (0.13 mmol, 0.1 equiv). The mixture was MW irradiated at 120 °C for 18 h. The crude mixture was extracted with DCM (30 mL) and washed with an aqueous solution of $NaHCO_3$ (3 × 20 mL). The organic layer was washed with brine (20 mL), dried over Na_2SO_4, filtered and the solvent was removed *in vacuo*.

The trifluoroacetamide intermediates (1 equiv) and potassium carbonate (2.5 equiv) in a mixture of MeOH (4 mL) and H_2O (0.30 mL) were refluxed for 1−3 h at 80 °C. The solvent was removed *in vacuo*. Water (30 mL) was added, and the aqueous solution was extracted with DCM (3 × 30 mL). The organic layer was dried with Na_2SO_4, filtered and concentrated *in vacuo*. The products **1** were purified with automated flash chromatography. Characterization data can be found in the Supporting Information.

Synthesis of Bisindole Secondary Amines 2

1a or **1b** (0.5 mmol) and the appropriate aldehyde (0.55 mmol, 1.1 equiv) were dissolved in MeOH (10 mL). Under an argon atmosphere at 0 °C, glacial acetic acid (2.3 mmol, 4.6 equiv) was added, and the reaction mixture was stirred for 30 min. $NaCNBH_3$ (1.3 mmol, 2.6 equiv) was then added, and the resulting mixture was stirred at rt for 3−24 h. The solvent was removed *in vacuo* and Na_2CO_3 (2 M in H_2O, 8 mL) was added to adjust the pH to 8−9. Water (30 mL) was added, and the reaction residue was extracted with DCM (3 × 30 mL). Organic phases were combined and washed with a solution of brine (20 mL), dried with Na_2SO_4, filtered and concentrated *in vacuo*. The products **2** were purified with automated

Downloaded from pubs.acs.org/aidcbc/article-pdf/12/9/3028/6733857/acsinfecdis.6c00079.pdf by UNIV DEGLI STUDI DI URBINO user on 15 September 2026

https://doi.org/10.1021/acsinfecdis.6c00079
ACS Infect. Dis. 2026, 12, 3028−3042

flash chromatography. Characterization data can be found in the Supporting Information.

Synthesis of Bisindole Amides 3

To a solution of the corresponding **1a** or **1b** (0.5 mmol, 0.075 M) and the appropriate carboxylic acid (0.53 mmol, 1.05 equiv) in dry DCM (6.7 mL), EDC hydrochloride (0.75 mmol, 1.5 equiv) was added at 0 °C. The reaction was then stirred at room temperature. After 12 h, the solution was quenched with sat. NH_4Cl aq. The resulting mixture was extracted with DCM (3 × 20 mL). The combined organic layers were dried over anhydrous Na_2SO_4, filtered, and concentrated *in vacuo*. The crude residue was purified by column chromatography on silica gel. Characterization data can be found in the Supporting Information.

Parasite and Cell Cultures

L. infantum MHOM/TN/80/IPT1 (WHO international reference strain) was purchased from ATCC (ATCC 50134) and the human monocytic cell line THP-1 (ECACC 88081201) were used in this study. Parasites were routinely cultured in Evans' Modified Tobie's Medium (EMTM) and maintained at 26 °C. For viability tests, parasites were cultivated in RPMI-PY medium supplemented as described by Castelli et al.[41] Human THP-1 cells were grown in RPMI-1640 medium supplemented with 10% fetal bovine serum (FBS), 100 μg/mL streptomycin and 100 U/mL penicillin at 37 °C with 5% CO_2 in a humidified incubator.

L. infantum Promastigotes and THP-1 Viability Assay

The activity of the bisindoles was initially assessed on 2.5 × 10^5 *L. infantum* late log/stationary phase promastigotesin 96-well plates (100 μL/well), at a single dose of 20 μM in triplicate for 72 h at 26 °C. Compounds displaying an inhibition greater than 60% were selected for a preliminary toxicity evaluation on THP-1 cells seeded at 5 × 10^5 cells/mL (100 μL/well) in 96-well plates and differentiated into macrophage-like cells with 20 ng/mL of phorbol 12-myristate 13-acetate (PMA) for 72 h. Cytotoxicity was investigated at 4 μM, 20 μM, and 100 μM to roughly determine the CC_{50} range. Compounds showing a half-maximal cytotoxic concentration (CC_{50}) > 20 μM were selected for the specific determination of half-maximal inhibitory concentration (IC_{50}) on parasites through dose−response curves. Briefly, promastigotes were treated with concentrations of each compound ranging from 20 μM to 0.3 μM (serial dilutions 1:2 and 2:3) for 72 h at 26 °C. Miltefosine, one of the reference drugs for leishmaniasis, was used as a positive control and tested under the same conditions. Each condition was carried out in duplicate. Parasite viability was determined using the CellTiter 96 AQueous Non-Radioactive Cell Proliferation Assay (Promega) as previously described[15] and the absorbance was measured at 492 nm using a microplate reader (Infinite F50 Plus, Tecan). To determine CC_{50} values, differentiated THP-1 cells were tested in duplicate, with compounds at concentrations ranging from 100 μM to 3.1 μM (1:2 dilutions) for 72 h at 37 °C. Miltefosine was used as positive control and tested under the same conditions. To assess the cytotoxicity of the compounds, the CellTiter 96 AQueous Non-Radioactive Cell Proliferation Assay (Promega) was employed as described above. The IC_{50} and CC_{50} values were calculated using nonlinear regression curves in GraphPad Prism 8.0 (GraphPad Software, Inc., San Diego, CA). The equation used for data fitting was $Y = 100/(1 + 10^{(\log IC50 - X) \times HillSlope})$ (hillslope not constrained), where X represents the logarithm of concentration and Y is the normalized response. For each compound, the SI was determined by calculating the ratio between the CC_{50} value in THP-1 cells and the IC_{50} value against *L. infantum* promastigotes.

Antiamastigote Assay on *L. infantum*-Infected THP-1 Cells

The activity of the primary amine **1e**, secondary amines **2b** and **2f**, and amides **3d** and **3e**, was further investigated in *L. infantum*-infected THP-1 cells. Specifically, THP-1 cells were seeded at a density of 3 × 10^5 cells per well in 12-well plates and differentiated into macrophage-like cells by treatment with 20 ng/mL PMA for 72 h. Following differentiation, late log/stationary phase *L. infantum* promastigotes were stained with carboxyfluorescein succinimidyl ester (CFSE), as previously described[24] and used to infect cells at a parasite-to-cell ratio of 10:1 for 24 h. After infection, noninternalized parasites were eliminated by replacing the culture medium. To accurately calculate the IC_{50} in intracellular amastigotes, infected cells were then treated for 72 h with the selected compounds at final concentrations of 1.25, 2, 5, 10, 15, and 20 μM. Miltefosine was used under the same conditions and included as positive control. Untreated infected cells were included as reference to normalize the infection rate. To calculate the magnitude of infection, cells were washed, fixed with 4% formaldehyde, permeabilized with methanol and finally stained with Hoechst dye. The stained cells were observed with a fluorescence microscope at 10× magnification. For each field, two images were acquired: one with excitation at 340−390 nm (for Hoechst dye) and the other with excitation at 460−495 nm (for CFSE). Automated cell counting of single-color images was performed with ImageJ software to monitor the rate of infection, which was determined by normalizing the amastigote count from each green (CFSE) image to the THP-1 cell count from the corresponding blue (Hoechst) image. At least 500 THP-1 cells were counted for each condition. The normalized infection rate for untreated infected cells was set as 100%.

Pharmacophore Model Building

A two-dimensional potential energy surface was generated for URB1483 and **2f** using a torsional scan procedure implemented in MacroModel.[42] The procedure was applied to dihedral angles τ_1 and τ_2 using 10 degrees incremental steps (Figure 3). The GB/SA implicit solvent model[43] with the OPLS4 force field[44] was adopted. **2f** was analyzed in both its neutral and protonated forms. Energy minimization was performed using the Polak-Ribière conjugate gradient method.[45] Convergence was set at 0.1 $kJ \cdot mol^{-1} \cdot Å^{-1}$. Considering common and nonredundant conformations in a 2 $kcal \cdot mol^{-1}$ window on the potential energy surfaces, four conformations of URB1483 and **2f** in neutral form were retrieved. Phase[46] was used to generate four pharmacophore models, each featuring five distinct sites:

(i) Two aromatic sites with a 2 Å radius were placed on the indole carbocycles (*aro1* and *aro2* sites in Figure 4). These sites are required for compounds to pass the screening filter.
(ii) One site was placed on the distal aromatic ring of URB1483's azole group (*nd-aro1* site), and another on the third aromatic ring of 2,2′-di(indol-3-yl)ethanamine derivatives (*nd-aro2* site). These sites, with varying radii of 2 Å and 1 Å, respectively, are considered optional during screening. Moreover, when scoring compounds, the directional component of the fitness score (i.e., vector score) was ignored for those sites.
(iii) Another site with a 1 Å radius was positioned on the secondary amine group of **2f** secondary amine group to accept positively charged groups (*pos1* site).

The pK_a of the secondary amine group of compound **2f** was calculated with the automated Jaguar workflow, which applies DFT calculations with empirical corrections to account for systematic errors in the implicit solvation energy.[47] Briefly, DFT calculations relied on ten conformers optimized at the B3LYP/cc-pVTZ//B3LYP/6-31G* level of theory, using the PCM implicit solvation model.[48]

To evaluate the pharmacophore models (I, II, III, and IV), ROC curves (Figure S7) were generated by screening 58 bisindole derivatives, which demonstrated activity in phenotypic screening against *Leishmania infantum* promastigote proliferation, against 3,550 (i.e., 50 inactive compounds for each of 71 prepared ligands) *bona fide* inactive decoys, retrieved from the DUD-E server.[49] The 58 derivatives included 12 compounds with azole-bisindole scaffold, from Diotallevi et al.,[23] 25 compounds from Centanni et al.[24] and 21 active compounds (**1b−e**, **2b−j** and **3c−j**) reported in this work.

Pharmacophore Screening

A list of proteins annotated for the *Leishmania* spp. and present in ChEMBL34[29] was utilized to identify a potential target for our compounds by identifying antileishmanial agents matching the

Downloaded from pubs.acs.org/aidcbc/article-pdf/12/9/3028/6733857/acsinfecdis.6c00079.pdf by UNIV DEGLI STUDI DI URBINO user on 15 September 2026

https://doi.org/10.1021/acsinfecdis.6c00079
ACS Infect. Dis. 2026, 12, 3028−3042

requirements of the pharmacophore models. Compounds with a *pChEMBL_value* greater than 5, corresponding to affinity or efficacy values below 10 μM, were selected. Additionally, only data with *assay_confidence_score* greater than 8 were considered to exclude compounds with undefined targets. This filtering process yielded a library of 508 compounds (Figure S8), which were prepared using LigPrep,[50] considering a pH range of 7.4 ± 1.0. The compounds were subjected to a pharmacophore screening with the four models (I, II, III and IV), using Phase.[46] Adherence to the two aromatic sites, corresponding to pharmacophore features occupied by indole rings, was prioritized by doubling the weight attributed to the vector score in the scoring function.

Docking Calculations

The crystal structure of TR of *L. infantum* (PDB ID 4ADW)[51] was prepared using the Protein Preparation workflow. Protonation states of ionizable residues were assigned using PropKa, accounting for the pH at which the crystal was obtained. The hydrogen bond network was optimized based on neighboring residues, and an *N*-methylamide group was added to the *C*-terminus. The refined structure underwent energy minimization to reduce steric strain until an energy gradient of 0.1 kJ·mol^{-1} was reached. Initially, heavy atoms were constrained, and subsequently, their RMSD deviation was restricted up to 0.3 Å from the starting structure.

The docking grid was centered on residues belonging to the catalytic tetrad (C52, C57, H461′, E466′) with bounding and enclosing boxes of 15 and 24 Å, respectively. Compound **6e**[30] (Table S1) was docked using Glide[52] in standard precision and the best pose according to docking score (Figure S11) was used to generate three aromatic sites to predict an initial pose of compound **2f**. This initial guess served as the basis to reconstruct the pharmacophore model of 2,2′-di(indol-3-yl)ethanamine derivatives and guide a ligand docking refinement protocol, similarly to previous calculations.[53]

TR Enzymatic Assay

LiTR has been expressed and purified as reported previously.[31,54] Enzymatic inhibition assays were performed in 50 mM HEPES buffer (pH 7.4), 40 mM NaCl, at 25 °C using a JASCO V650 spectrophotometer equipped with a JASCO EHC-716 Peltier element to ensure controlled temperature. An initial experiment was carried out with 50 nM LiTR, 10 μM of the test compound (resulting in a 1% DMSO concentration in the reaction mix), 150 μM trypanothione disulfide (purchased from Bachem), and 100 μM NADPH tetrasodium salt (purchased from Calbiochem).

The most promising inhibitor candidate **2f** was then tested at concentrations ranging from 1 nM to 250 μM in order to determine the IC_{50}. Assays were initiated by the addition of 100 μM NADPH to 50 nM LiTR in the presence of various concentrations of the compounds and 150 μM trypanothione. In both cases, NADPH oxidation was monitored as a decrease in absorbance at 340 nm. For each compound concentration, the initial velocity of NADPH oxidation was used to calculate the percentage of LiTR activity relative to that in the absence of inhibitor. The IC_{50} was determined by fitting the residual TR activity to a dose−response logistic equation defined as $y = y_{min} + (y_{max} - y_{min})/(1 + (x/IC_{50})^{slope})$. Data analysis was performed with QtiPlot 0.9.8.9 svn 2288, and graphs were generated using Matplotlib.[31]

Statistical Analysis

The calculation of IC_{50} in promastigotes and CC_{50} in human cells following the treatments was performed by nonlinear regression analysis and expressed as mean and 95% confidence interval. Statistical evaluation of treatment efficacy on amastigotes was performed using one-way ANOVA, followed by Tukey's multiple comparisons test. All statistical analyses were conducted using GraphPad Prism version 8 and a p-value ≤ 0.05 was considered significant.

Developability and ADME-Related Studies

Materials and methods for kinetic solubility, chemical and metabolic stabilities are reported in the Supporting Information.

ASSOCIATED CONTENT

Supporting Information

The Supporting Information is available free of charge at https://pubs.acs.org/doi/10.1021/acsinfecdis.6c00079.

Materials for chemistry; experimental data for compounds **1**, **2**, and **3**; ^{1}H NMR and ^{13}C NMR spectra; dose−response curves of **1e**, **2b**, **2c**, **2f**, **2i**, **2j**, **3d**, and **3e** on *L. infantum* MHOM/TN/80/IPT1 promastigotes (Figure S1); dose−response curves of **1e**, **2b**, **2c**, **2f**, **2i**, **2j**, **3d**, and **3e** on THP-1 cells (Figure S2); cytotoxic effect of treatment with **2f** on infected (amastigotes) THP-1 cells (Figure S3); potential energy surfaces of URB1483 and **2f** (Figures S4−S5); conformational parameters of compound **2f** (Figure S6); receiver operating characteristic curves evaluated for pharmacophore models (Figure S7); pharmacophore screening of antileishmanial agents for target fishing (Figures S8−S11 and Table S1); evaluation of LiTR enzymatic inhibition (Figures S12−S13); chemical stability of compounds **1e** and **2f** in phosphate buffer (Figure S14); plasma stability of URB1483, **1e**, and **2f** (Table S2); metabolic stability of URB1483 in HLM (Figure S15); materials and methods for developability and ADME-related studies (PDF)

AUTHOR INFORMATION

Corresponding Author

Simone Lucarini − *Department of Biomolecular Sciences, University of Urbino Carlo Bo, Urbino 61029, Italy;* orcid.org/0000-0002-3667-1207; Phone: +390722303333; Email: simone.lucarini@uniurb.it

Authors

Gian Marco Elisi − *Department of Biomolecular Sciences, University of Urbino Carlo Bo, Urbino 61029, Italy;* orcid.org/0000-0001-9071-5621

Antonio Gkoutzamanis − *Drug Research Program, Division of Pharmaceutical Chemistry and Technology, Faculty of Pharmacy, University of Helsinki, Helsinki 00014, Finland*

Sara Maestrini − *Department of Biomolecular Sciences, University of Urbino Carlo Bo, Urbino 61029, Italy*

Cécile Exertier − *Institute of Molecular Biology and Pathology (IBPM) of the Italian National Research Council (CNR), C/O Department of Biochemical Sciences "A. Rossi Fanelli", Sapienza University of Roma, Rome 00185, Italy;* orcid.org/0000-0001-7457-6895

Michela Eleuteri − *DAISY Lab (Drug Discovery-Artificial Intelligence-Organic Synthesis), Department of Chemistry, Biology and Biotechnology, University of Perugia, Perugia 06123, Italy*

Marina Naldi − *Bio-Pharmaceutical and Pharmaceutical Analysis Lab, Department of Pharmacy and Biotechnology, Alma Mater Studiorum University of Bologna, Bologna 40126, Italy*

Alessia Peluso − *Department of Biomolecular Sciences, University of Urbino Carlo Bo, Urbino 61029, Italy*

Miriam Gómez-Benmansour − *Department of Biomolecular Sciences, University of Urbino Carlo Bo, Urbino 61029, Italy;* orcid.org/0009-0002-0541-2816

Downloaded from pubs.acs.org/aidcbc/article-pdf/12/9/3028/6733885/7/acsinfecdis.6c00079.pdf by UNIV DEGLI STUDI DI URBINO user on 15 September 2026

Aurora Diotallevi − *Department of Biomolecular Sciences, University of Urbino Carlo Bo, Urbino 61029, Italy;* orcid.org/0000-0001-5456-1821
Michele Verboni − *Department of Biomolecular Sciences, University of Urbino Carlo Bo, Urbino 61029, Italy*
Laura Goracci − *DAISY Lab (Drug Discovery-Artificial Intelligence-Organic Synthesis), Department of Chemistry, Biology and Biotechnology, University of Perugia, Perugia 06123, Italy;* orcid.org/0000-0002-9282-9013
Manuela Bartolini − *Bio-Pharmaceutical and Pharmaceutical Analysis Lab, Department of Pharmacy and Biotechnology, Alma Mater Studiorum University of Bologna, Bologna 40126, Italy;* orcid.org/0000-0002-2890-3856
Giovanni Bottegoni − *Department of Biomolecular Sciences, University of Urbino Carlo Bo, Urbino 61029, Italy; School of Pharmacy, University of Birmingham, Birmingham B15 2TT, U.K.;* orcid.org/0000-0003-1251-583X
Paula Kiuru − *Drug Research Program, Division of Pharmaceutical Chemistry and Technology, Faculty of Pharmacy, University of Helsinki, Helsinki 00014, Finland;* orcid.org/0000-0001-6084-684X
Andrea Ilari − *Institute of Molecular Biology and Pathology (IBPM) of the Italian National Research Council (CNR), C/O Department of Biochemical Sciences "A. Rossi Fanelli", Sapienza University of Roma, Rome 00185, Italy;* orcid.org/0000-0002-7754-399X
Luca Galluzzi − *Department of Biomolecular Sciences, University of Urbino Carlo Bo, Urbino 61029, Italy;* orcid.org/0000-0002-1747-526X

Complete contact information is available at: https://pubs.acs.org/10.1021/acsinfecdis.6c00079

Author Contributions

Conceptualization: G.M.E., L.Ga., and S.L.; data curation: G.M.E., A.D., L.Go., M.B., P.K., A.I., and L.Ga.; funding acquisition: G.B., L.Ga., and S.L.; investigation: G.M.E., A.G., S.M., C.E., M.E., M.N., A.P., M.G.B., A.D., and M.V.; methodology: G.M.E., A.D., M.V., P.K., and A.I.; project administration: G.B., L.Ga., and S.L.; supervision: L.Go., P.K., A.I., L.Ga., and S.L.; writing—original draft: G.M.E. and S.L.; writing—review and editing: G.M.E., S.M., C.E., M.E., A.D., L.Go., M.B., P.K., A.I., L.Ga., and S.L. All authors have given approval to the final version of the manuscript.

Funding

This work has been funded by the European Union_-NextGenerationEU, Mission 4, Component 2, under the Italian Ministry of University and Research (MUR) National Innovation Ecosystem grant ECS00000041_VITALITY_CUP H33C22000430006 and CUP J13C22000430001, and by FanoAteneo. Moreover, it has been funded by "Potentiating the Italian Capacity for Structural Biology Services in Instruct ERIC (ITACA.SB)" (Project No. IR0000009) within the call MUR 3264/2021 PNRR M4/C2/L3.1.1, funded by the European Union NextGenerationEU and Collezione di Composti Chimici ed Attività di Screening (CNCCS) DSB.AD011.013.001, FOE 2024.

Notes

The authors declare no competing financial interest.

ACKNOWLEDGMENTS

The authors thank Prof. Michele Menotta (University of Urbino Carlo Bo) and Dr. Nina Sipari (Viikki Metabolomics Unit, University of Helsinki) for HRMS characterization of the new compounds.

ABBREVIATIONS

CI, confidence interval; CL, cutaneous leishmaniasis; DCM, dichloromethane; DMSO, dimethyl sulfoxide; DPP, diphenyl phosphate; EDC, *N*-(3-(dimethylamino)propyl)-*N*′-ethylcarbodiimide; ESI, electrospray ionization; FaSSIF, fasted-state simulated intestinal fluid; FeSSIF, fed-state simulated intestinal fluid; HLM, human liver microsomes; HRMS, high-resolution mass spectrometry; LC-MS, liquid chromatography−mass spectrometry; LiTR, *Leishmania infantum* trypanothione reductase; MILT, miltefosine; MW, microwave; PDB, Protein Data Bank; PK, Pharmacokinetic; ROC, receiver operating characteristic; SD, standard deviation; SI, selectivity index; THF, tetrahydrofuran; TR, trypanothione reductase; VL, visceral leishmaniasis

REFERENCES

(1) Nagle, A. S.; Khare, S.; Kumar, A. B.; Supek, F.; Buchynskyy, A.; Mathison, C. J.; Chennamaneni, N. K.; Pendem, N.; Buckner, F. S.; Gelb, M. H.; Molteni, V. Recent developments in drug discovery for leishmaniasis and human African trypanosomiasis. *Chem. Rev.* **2014**, *114*, 11305−11347.
(2) Gupta, O.; Pradhan, T.; Bhatia, R.; Monga, V. Recent advancements in anti-leishmanial research: Synthetic strategies and structural activity relationships. *Eur. J. Med. Chem.* **2021**, *223*, 113606.
(3) Pal, R.; Teli, G.; Akhtar, J.; Matada, J.; Matada, G. S. P. Synthetic product-based approach toward potential antileishmanial drug development. *Eur. J. Med. Chem.* **2024**, *263*, 115927.
(4) World Health Organization (WHO) official web page on Leishmaniasis: https://www.who.int/news-room/fact-sheets/detail/leishmaniasis (accessed on 7 January 2026).
(5) Di Muccio, T.; Scalone, A.; Bruno, A.; Marangi, M.; Grande, R.; Armignacco, O.; Gradoni, L.; Gramiccia, M. Epidemiology of imported leishmaniasis in Italy: implications for a European endemic country. *PLoS One* **2015**, *10*, No. e0129418.
(6) Todeschini, R.; Musti, M. A.; Pandolfi, P.; Troncatti, M.; Baldini, M.; Resi, D.; Natalini, S.; Bergamini, F.; Galletti, G.; et al. Reemergence of human leishmaniasis in northern Italy, 2004 to 2022: a retrospective analysis. *Euro Surveill* **2023**, *29* (4), 2300190.
(7) Pace, D. Leishmaniasis. *J. Infect* **2014**, *69*, S10−S18.
(8) Barbiero, A.; Spinicci, M.; Aiello, A.; Maruotto, M.; Antonello, R. M.; Formica, G.; Piccica, M.; Isola, P.; Parisio, E. M.; Nardone, M.; Valentini, S.; Mangano, V.; Brunelli, T.; Bianchi, L.; Bartalesi, F.; Costa, C.; Sambo, M.; Tumbarello, M.; Sani, S.; Fabiani, S.; Rossetti, B.; Nencioni, C.; Lanari, A.; Aquilini, D.; Montorzi, G.; Venturini, E.; Galli, L.; Rinninella, G.; Falcone, M.; Ceriegi, F.; Amadori, F.; Vincenti, A.; Blanc, P.; Vellere, I.; Tacconi, D.; Luchi, S.; Moneta, S.; Massi, D.; Brogi, M.; Voller, F.; Gemmi, F.; Rossolini, G. M.; Cusi, M. G.; Bruschi, F.; Bartoloni, A.; Zammarchi, L. The Uprise of Human Leishmaniasis in Tuscany, Central Italy: Clinical and Epidemiological Data from a Multicenter Study. *Microorganisms* **2024**, *12*, 1963.
(9) Srivastava, S.; Shankar, P.; Mishra, J.; Singh, S. Possibilities and challenges for developing a successful vaccine for leishmaniasis. *Parasit. Vectors* **2016**, *9*, 277.
(10) Ponte-Sucre, A.; Gamarro, F.; Dujardin, J.-C.; Barrett, M. P.; López-Vélez, R.; García-Hernández, R.; Pountain, A. W.; Mwenechanya, R.; Papadopoulou, B. Drug resistance and treatment failure in leishmaniasis: A 21st century challenge. *PLoS Negl. Trop. Dis.* **2017**, *11*, No. e0006052.
(11) Razzaghi-Asl, N.; Sepehri, S.; Ebadi, A.; Karami, P.; Nejatkhah, N.; Johari-Ahar, M. Insights into the current status of privileged *N*-

Downloaded from pubs.acs.org/aidcbc/article-pdf/12/9/3028/6733857/acsinfecdis.6c00079.pdf by UNIV DEGLI STUDI DI URBINO user on 15 September 2026

heterocycles as antileishmanial agents. *Mol. Diversity* **2020**, *24*, 525−569.
(12) Verboni, M.; Olivieri, D.; Lucarini, S. A recent update on new synthetic chiral compounds with antileishmanial activity. *Chirality* **2022**, *34*, 1279−1297.
(13) Bekhit, A. A.; El-Agroudy, E.; Helmy, A.; Ibrahim, T. M.; Shavandi, A.; Bekhit, A. E.-D. A. Leishmania treatment and prevention: natural and synthesized drugs. *Eur. J. Med. Chem.* **2018**, *160*, 229−244.
(14) Rathore, S.; Sahu, A.; Agrawal, R. K.; Patil, A. G. A critical review on recent heterocyclics identified for anti-leishmanial therapy. *Current Chem. Biol.* **2022**, *16*, 81−105.
(15) Ciccone, V.; Diotallevi, A.; Gómez-Benmansour, M.; Maestrini, S.; Mantellini, F.; Mari, G.; Galluzzi, L.; Lucarini, S.; Favi, G. Easy one-pot synthesis of multifunctionalized indole-pyrrole hybrids as a new class of antileishmanial agents. *RSC Adv.* **2024**, *14*, 15713−15720.
(16) Sangshetti, J. N.; Kalam Khan, F. A.; Kulkarni, A. A.; Arote, R.; Patil, R. H. Antileishmanial drug discovery: comprehensive review of the last 10 years. *RSC Adv.* **2015**, *5*, 32376−32415.
(17) Roy, A.; Das, B. B.; Ganguly, A.; Dasgupt, S. B.; Khalkho, N. V. M.; Pal, C.; Dey, S.; Giri, V. S.; Jaisankar, P.; Dey, S.; et al. An insight into the mechanism of inhibition of unusual bi-subunit topoisomerase I from Leishmania donovani by 3,3′-di-indolylmethane, a novel DNA topoisomerase I poison with a strong binding affinity to the enzyme. *Biochem. J.* **2008**, *409*, 611−622.
(18) Roy, A.; Chowdhury, S.; Sengupta, S.; Mandal, M.; Jaisankar, P.; D'Annessa, I.; Desideri, A.; Majumder, H. K. Development of derivatives of 3,3′-diindolylmethane as potent *Leishmania donovani* bi-subunit Topoisomerase IB poisons. *PLoS One* **2011**, *6*, No. e28493.
(19) Bharate, S. B.; Bharate, J. B.; Khan, S. I.; Tekwani, B. L.; Jacob, M. R.; Mudududdla, R.; Yadav, R. R.; Singh, B.; Sharma, P. R.; Maity, S.; Singh, B.; Khan, I. A.; Vishwakarma, R. A. Discovery of 3,3′-diindolylmethanes as potent antileishmanial agents. *Eur. J. Med. Chem.* **2013**, *63*, 435−443.
(20) Khan, F. A. K.; Zaheer, Z.; Sangshetti, J. N.; Patil, R. H.; Farooqui, M. Antileishmanial evaluation of clubbed bis(indolyl)-pyridine derivatives: one-pot synthesis, *in vitro* biological evaluations and in silico ADME prediction. *Bioorg. Med. Chem. Lett.* **2017**, *27*, 567−573.
(21) Taha, M.; Uddin, I.; Gollapalli, M.; Almandil, N. B.; Rahim, F.; Farooq, R. K.; Nawaz, M.; Ibrahim, M.; Alqahtani, M. A.; Bamarouf, Y. A.; et al. Synthesis, anti-leishmanial and molecular docking study of bis-indole derivatives. *BMC Chem.* **2019**, *13*, 102.
(22) Kour, P.; Saha, P.; Bhattacharya, S.; Kumari, D.; Debnath, A.; Roy, A.; Sharma, D. K.; Mukherjee, D.; Singh, K. Design, synthesis, and biological evaluation of 3,3′-diindolylmethane N-linked glyco-conjugate as a leishmanial topoisomerase IB inhibitor with reduced cytotoxicity. *RSC Med. Chem.* **2023**, *14*, 2100−2114.
(23) Diotallevi, A.; Scalvini, L.; Buffi, G.; Pérez-Pertejo, Y.; De Santi, M.; Verboni, M.; Favi, G.; Magnani, M.; Lodola, A.; Lucarini, S.; Galluzzi, L. Phenotype screening of an azole-bisindole chemical library identifies URB1483 as a new antileishmanial agent devoid of toxicity on human cells. *ACS Omega* **2021**, *6* (51), 35699−35710.
(24) Centanni, A.; Diotallevi, A.; Buffi, G.; Olivieri, D.; Santarém, N.; Lehtinen, A.; Yli-Kauhaluoma, J.; Cordeiro-da-Silva, A.; Kiuru, P.; Lucarini, S.; Galluzzi, L. Exploring hydrophilic 2,2-di(indol-3-yl)ethanamine derivatives against *Leishmania infantum*. *PLoS One* **2024**, *19*, No. e0301901.
(25) Buono, A.; Diotallevi, A.; Maestrini, S.; Verboni, M.; Kiuru, P.; Galluzzi, L.; Duranti, A.; Olivieri, D.; Lucarini, S. Efficient and rapid arylation of NH_2-unprotected bromobisindole ethanamines via Suzuki-Miyaura coupling: Generating new leads against Leishmania. *Chem.—Eur. J.* **2025**, *31*, No. e202500637.
(26) Zivanovic, S.; Colizzi, F.; Moreno, D.; Hospital, A.; Soliva, R.; Orozco, M. Exploring the conformational landscape of bioactive small molecules. *J. Chem. Theory Comput.* **2020**, *16* (10), 6575−6585.
(27) Elisi, G. M.; Bedini, A.; Scalvini, L.; Carmi, C.; Bartolucci, S.; Lucini, V.; Scaglione, F.; Mor, M.; Rivara, S.; Spadoni, G. Chiral recognition of flexible melatonin receptor ligands induced by conformational equilibria. *Molecules* **2020**, *25* (18), 4057.
(28) Battista, T.; Colotti, G.; Ilari, A.; Fiorillo, A. Targeting trypanothione reductase, a key enzyme in the redox trypanosomatid metabolism, to develop new drugs against leishmaniasis and trypanosomiases. *Molecules* **2020**, *25* (8), 1924.
(29) Zdrazil, B.; Felix, E.; Hunter, F.; Manners, E. J.; Blackshaw, J.; Corbett, S.; de Veij, M.; Ioannidis, H.; Lopez, D. M.; Mosquera, J. F.; Magarinos, M. P.; Bosc, N.; Arcila, R.; Kiziloren, T.; Gaulton, A.; Bento, A. P.; Adasme, M. F.; Monecke, P.; Landrum, G. A.; Leach, A. R. The ChEMBL Database in 2023: a drug discovery platform spanning multiple bioactivity data types and time periods. *Nucleic Acids Res.* **2024**, *52*, D1180−D1192.
(30) Chauhan, S. S.; Pandey, S.; Shivahare, R.; Ramalingam, K.; Krishna, S.; Vishwakarma, P.; Siddiqi, M. I.; Gupta, S.; Goyalc, N.; Chauhan, P. M. S. Novel β-carboline-quinazolinone hybrid as an inhibitor of Leishmania donovani trypanothione reductase: Synthesis, molecular docking and bioevaluation. *MedChemComm* **2015**, *6* (2), 351−356.
(31) Exertier, C.; Salerno, A.; Antonelli, L.; Fiorillo, A.; Ocello, R.; Seghetti, F.; Caciolla, J.; Uliassi, E.; Masetti, M.; Fiorentino, E.; Orsini, S.; Di Muccio, T.; Ilari, A.; Bolognesi, M. L. Fragment merging, growing, and linking identify new trypanothione reductase inhibitors for leishmaniasis. *J. Med. Chem.* **2024**, *67*, 402−419.
(32) Venturi, A.; Di Bona, S.; Desantis, J.; Eleuteri, M.; Bartalucci, M.; Baroni, M.; Benedetti, P.; Goracci, L.; Cruciani, G. Between theory and practice: Computational/experimental integrated approaches to understand the solubility and lipophilicity of PROTACs. *J. Med. Chem.* **2024**, *67* (18), 16355−16380.
(33) Laizure, S. C.; Herring, V.; Hu, Z.; Witbrodt, K.; Parker, R. B. The role of human carboxylesterases in drug metabolism: have we overlooked their importance? *Pharmacotherapy* **2013**, *33* (2), 210−222.
(34) Bonn, B.; Leandersson, C.; Fontaine, F.; Zamora, I. Enhanced metabolite identification with MS^E and a semi-automated software for structural elucidation. *Rapid Commun. Mass Spectrom.* **2010**, *24*, 3127−3138.
(35) Zamora, I.; Fontaine, F.; Serra, B.; Plasencia, G. High-throughput, computer assisted, specific MetID. A revolution for drug discovery. *Drug Discov. Today* **2013**, *10* (1), No. e199−e205.
(36) Strano-Rossi, S.; Anzillotti, L.; Dragoni, S.; Pellegrino, R. M.; Goracci, L.; Pascali, V. L.; Cruciani, G. Metabolism of JWH-015, JWH-098, JWH-251, and JWH-307 *in silico* and *in vitro*: A pilot study for the detection of unknown synthetic cannabinoids metabolites. *Anal. Bioanal. Chem.* **2014**, *406*, 3621−3636.
(37) Brink, A.; Fontaine, F.; Marschmann, M.; Steinhuber, B.; Cece, E. N.; Zamora, I.; Pähler, A. Post-acquisition analysis of untargeted accurate mass quadrupole time-of-flight MS^E data for multiple collision-induced neutral losses and fragment ions of glutathione conjugates. *Rapid Commun. Mass Spectrom.* **2014**, *28*, 2695−2703.
(38) Radchenko, T.; Fontaine, F.; Morettoni, L.; Zamora, I. WebMetabase: cleavage sites analysis tool for natural and unnatural substrates from diverse data source. *Bioinformatics* **2019**, *35* (4), 650−655.
(39) Borsari, C.; Santarem, N.; Coertzen, D.; Mazzolari, A.; Corfu, A. I.; Coelho, C.; Barbosa, F.; Tamborini, L.; Birkholtz, L.-M.; Raffellini, L.; Keminer, O.; Basilico, N.; Parapini, S.; Gul, S.; Cordeiro-da-Silva, A.; Conti, P. From pan-active to parasite-selective antiparasitic agents: A scaffold hopping approach. *Eur. J. Med. Chem.* **2025**, *300*, 118095.
(40) Mano, C.; Kongkaew, A.; Tippawangkosol, P.; Somboon, P.; Roytrakul, S.; Pescher, P.; Späth, G. F.; Uthaipibull, C.; Tantiworawit, A.; Siriyasatien, P.; Jariyapan, N. Amphotericin B resistance correlates with increased fitness *in vitro* and *in vivo* in Leishmania (Mundinia) martiniquensis. *Front. Microbiol.* **2023**, *14*, 1156061.
(41) Castelli, G.; Galante, A.; Verde, V. L.; Migliazzo, A.; Reale, S.; Lupo, T.; Piazza, M.; Vitale, F.; Bruno, F. Evaluation of two modified culture media for *Leishmania infantum* cultivation versus different culture media. *J. Parasitol.* **2014**, *100*, 228−230.

Downloaded from pubs.acs.org/aidcbc/article-pdf/12/9/3028/6733857/acsinfecdis.6c00079.pdf by UNIV DEGLI STUDI DI URBINO user on 15 September 2026

https://doi.org/10.1021/acsinfecdis.6c00079
ACS Infect. Dis. 2026, 12, 3028−3042

(42) *Schrödinger Release 2023−4: MacroModel* ; Schrödinger, LLC: New York, NY, 2023.
(43) Still, W. C.; Tempczyk, A.; Hawley, R. C. Semianalytical treatment of solvation for molecular mechanics and dynamics. *J. Am. Chem. Soc.* **1990**, *112*, 6127−6129.
(44) Lu, C.; Wu, C.; Ghoreishi, D.; Chen, W.; Wang, L.; Damm, W.; Ross, G.; Dahlgren, M.; Russell, E.; Von Bargen, C.; Abel, R.; Friesner, R.; Harder, E. OPLS4: Improving force field accuracy on challenging regimes of chemical space. *J. Chem. Theory Comput.* **2021**, *17*, 4291−4300.
(45) Polak, E.; Ribière, G. Note sur la convergence de méthodes de directions conjuguées. *ESAIM Math. Model. Numer. Anal. Modél. Math. Anal. Numér.* **1969**, *3*, 35−43.
(46) *Schrödinger Release 2023−4: phase*; Schrödinger, LLC, New York, NY, 2023.
(47) Bochevarov, A. D.; Watson, M. A.; Greenwood, J. R.; Philipp, D. M. Multiconformation, density functional theory-based pKa prediction in application to large, flexible organic molecules with diverse functional groups. *J. Chem. Theory Comput.* **2016**, *12*, 6001−6019.
(48) Tomasi, J.; Mennucci, B.; Cammi, R. Quantum Mechanical Continuum Solvation Models. *Chem. Rev.* **2005**, *105*, 2999−3094.
(49) Mysinger, M. M.; Carchia, M.; Irwin, J. J.; Schoichet, B. K. Directory of useful decoys, enhanced (DUD-E): Better ligands and decoys for better benchmarking. *J. Med. Chem.* **2012**, *55* (14), 6582−6594.
(50) *Schrödinger Release 2023−4: LigPrep*; Schrödinger, LLC: New York, NY, 2023.
(51) Baiocco, P.; Poce, G.; Alfonso, S.; Cocozza, M.; Porretta, G. C.; Colotti, G.; Biava, M.; Moraca, F.; Botta, M.; Yardley, V.; Fiorillo, A.; Lantella, A.; Malatesta, F.; Ilari, A. Inhibition of Leishmania infantum trypanothione reductase by azole-based compounds: a comparative analysis with its physiological substrate by X-ray crystallography. *ChemMedChem* **2013**, *8* (7), 1175−1183.
(52) Friesner, R. A.; Banks, J. L.; Murphy, R. B.; Halgren, T. A.; Klicic, J. J.; Mainz, D. T.; Repasky, M. P.; Knoll, E. H.; Shelley, M.; Perry, J. K.; Shaw, D. E.; Francis, P.; Shenkin, P. S. Glide: A new approach for rapid, accurate docking and scoring. 1. Method and assessment of docking accuracy. *J. Med. Chem.* **2004**, *47*, 1739−1749.
(53) Caputo, A.; Elisi, G. M.; Levati, E.; Barotti, G.; Sartini, S.; Wagner, J.; Burnouf, D. Y.; Ottonello, S.; Rivara, S.; Montanini, B. Small molecules targeting the eubacterial β-sliding clamp discovered by combined *in silico* and *in vitro* screening approaches. *J. Enzyme Inhib. Med. Chem.* **2025**, *40* (1), 2440861.
(54) Baiocco, P.; Franceschini, S.; Ilari, A.; Colotti, G. Trypanothione reductase from Leishmania infantum: Cloning, expression, purification, crystallization and preliminary X-ray data analysis. *Protein Pept. Lett.* **2009**, *16* (2), 196−200.

Downloaded from pubs.acs.org/aidcbc/article-pdf/12/9/3028/6733885/7/acsinfecdis.6c00079.pdf by UNIV DEGLI STUDI DI URBINO user on 15 September 2026

https://doi.org/10.1021/acsinfecdis.6c00079
ACS Infect. Dis. 2026, 12, 3028−3042